NACA

RESEARCH MEMORANDUM

CLASSIFICATION CANCELLED
AUTHORITY H.L. DRYDEN   CHANGE #1412
DATE 6-5-53   T.C. FRASER, JR.

EFFECTS OF COMPRESSIBILITY ON THE CHARACTERISTICS

OF FIVE AIRFOILS

By

Bernard N. Daley

Langley Memorial Aeronautical Laboratory
Langley Field, Va.

CLASSIFIED DOCUMENT

This document contains classified information affecting the National Defense of the United States within the meaning of the Espionage Act, USC 50:31 and 32. Its transmission or the revelation of its contents in any manner to an unauthorized person is prohibited by law. Information so classified may be imparted only to persons in the military and naval services of the United States, appropriate civilian officers and employees of the Federal Government who have a legitimate interest therein, and to United States citizens of known loyalty and discretion who of necessity must be informed thereof.

NATIONAL ADVISORY COMMITTEE
FOR AERONAUTICS

WASHINGTON
April 25, 1947

CONFIDENTIAL

NATIONAL ADVISORY COMMITTEE FOR AERONAUTICS

RESEARCH MEMORANDUM

EFFECTS OF COMPRESSIBILITY ON THE CHARACTERISTICS

OF FIVE AIRFOILS

By Bernard N. Daley

SUMMARY

Pressure-distribution tests were made for determination of the effects of compressibility on the characteristics of the following 5-inch-chord airfoils: the NACA 66,2-215, the NACA 66,2-015, and the NACA 65(216)-418 sections representing the low-drag sections; the NACA 16-212 section, typical of the type designed for high critical speeds; and the NACA 23015 section, one of the older conventional airfoils. Schlieren photographs of the air flow and limited data concerning the wake characteristics were also obtained for the conventional airfoil. Data are presented for an approximate Mach number range from 0.34 to 0.75; the corresponding Reynolds number range is from 700,000 to 1,800,000.

The results illustrate the general nature of the effects of compressibility on the flow. The schlieren photographs showed that for constant moderate angles of attack pronounced separation of the flow occurred from only one surface of the NACA 23015 airfoil at supercritical speeds. The data from the wake surveys showed that this separation produced large variations with Mach number of the location of the center of the wake. It was shown that the camber of the wing section should be carefully selected to insure high values of the critical speed of the wing section at any design condition. The Mach number increment between the critical Mach number and the Mach number of the normal-force break is shown to be closely related to the location of the low-speed maximum negative pressure coefficient. At small angles of attack this increment was approximately 0.13 for the NACA 23015 airfoil and 0.03 for the newer type airfoil sections. A shift in the angle of zero lift was shown to occur at high Mach numbers for all the newer cambered airfoils tested. This shift is attributed to flow separation and to the decreased influence of any disturbance on the oncoming stream. A positive trend for the change of pitching moment coefficient with normal-force coefficient was found for all the newer airfoils tested with increasing Mach number, whereas the trend for the NACA 23015 airfoil with increasing Mach number was negative.

INTRODUCTION

As a consequence of the many uncertainties in the nature of air flow at high speeds, theoretical considerations of the effects of compressibility on bodies have been limited in scope to several basic shapes and subcritical Mach numbers. Experimental data are being relied upon almost completely to determine the magnitude and effect of shock phenomena. The need for experimental data therefore is great. References 1, 2, and 3 are representative of previous experimental data. Force measurements, wake-survey data, pressure-distribution diagrams, and schlieren photographs obtained under similar test conditions are presented in reference 1. These data were obtained from older conventional airfoils and similar data are needed for the newer low-drag and high-speed type airfoils.

The purpose of this investigation was to provide data to illustrate the effects of compressibility on the characteristics of airfoils of the newer low-drag type, the high-critical-speed type, and the older conventional type.

SYMBOLS

α angle of attack, degrees

c_n airfoil section normal-force coefficient

$c_{m_{c/4}}$ airfoil section quarter-chord pitching-moment coefficient

M stream Mach number

M_{cr} stream Mach number at which the local velocity of sound is attained

M_{lb} stream Mach number at which a rapid change in the normal-force characteristic originates

ΔM increment in Mach number $\left(M_{lb} - M_{cr} \right)$

p_l local static pressure

p_s stream static pressure

P pressure coefficient $\left(\dfrac{p_l - p_s}{q} \right)$

P_{cr} pressure coefficient corresponding to the local velocity of sound

P_{max} maximum pressure coefficient

q stream dynamic pressure

$\dfrac{\partial c_{m_{c/4}}}{\partial c_n}$ rate of change of moment coefficient with normal-force coefficient

$\dfrac{\partial c_{m_{c/4}}}{\partial \alpha}$ rate of change of moment coefficient with angle of attack

$\dfrac{\partial c_n}{\partial \alpha}$ rate of change of normal-force coefficient with angle of attack

APPARATUS AND METHODS

Tunnel.- All the tests were made in the Langley rectangular high-speed tunnel. This tunnel is of the closed-throat, nonreturn, induction type, which utilizes air at high pressure in an annular nozzle downstream of the test section to induce an air flow through the tunnel. The height of the test section is 18 inches and the width 4 inches. For complete description of this type wind tunnel see figure 1 and reference 1.

Flexible steel walls 4 inches wide constitute two of the boundaries and heavy fixed steel plates form the other boundaries. Although the flexible walls permit an adjustment of the longitudinal static-pressure gradient of the tunnel so that a Mach number up to approximately 1.4 is possible, the flexible walls for the present tests were set to maintain a fairly uniform longitudinal static-pressure gradient through the test section at any Mach number below 0.85 with tunnel empty.

The airfoil models completely spanned the 4-inch dimension of the tunnel and were supported by end plates in the fixed walls. This arrangement eliminated strut interference and end-gap effects.

Models.- The following airfoil sections were used in this investigation:

NACA 23015	an older conventional section in wide use
NACA 16-212	one of a type designed for high critical speeds
NACA 66,2-215	a low-drag type section for use in a pursuit airplane
NACA 66,2-015	a low-drag section for possible use in a pursuit airplane
NACA 65(216)-418	a low-drag section for possible use in a bomber

Each model of 4-inch span and 5-inch chord was fitted with about thirty-five 0.008-inch-diameter orifices distributed over the surface in a region within 1/4 inch from the semispan or center line of the tunnel. About 20 of these orifices were on the upper surface. In order to eliminate interference, all pressure leads were taken from the ends of the model through the end plates.

Optical equipment.- A description of the optical setup for obtaining schlieren photographs is presented in reference 1. This method of photography utilizes the principle of change in index of refraction of air with change in density. Shock waves and other similar disturbances are accompanied by a change in density at the position of the disturbance and a corresponding light or dark region therefore appears on the photograph. When schlieren photographs were taken, the airfoil model was supported by means of dowels in glass end plates. In this way, any interference to the air stream or obstructions in the photographic field were eliminated.

TESTS

Airfoil sections were tested which are representative of those either in use or considered for use. In this group are included the NACA 230-series, the NACA 16-series, and the NACA 6-series type of airfoil. Profiles and ordinates of these airfoils are presented in figure 2 and table 1, respectively. Pressure-distribution tests were made on each of the 5-inch-chord models previously mentioned. Schlieren photographs were made of the NACA 23015 profile at supercritical speeds.

All tests were made at constant angles of attack over the speed range. The airfoil models were mounted with the quarter-chord location coinciding with the center of the end plate. The angle-of-attack range was from -4° to 6°. The test results are presented for a Mach number range extending from 0.34 to approximately 0.75. The Mach number was determined from the pressure measured at a calibrated static-pressure orifice $5\frac{3}{4}$ inches upstream of the leading edge of the model. The Reynolds numbers corresponding to this Mach number range vary from 700,000 to 1,800,000.

PRECISION

<u>Constriction and choking</u>.- Experimental data from both the Langley 24-inch high-speed tunnel (reference 4) and the Langley rectangular high-speed tunnel indicate the presence of tunnel-wall constriction. The nature of this constriction is best illustrated at the choked condition, the maximum speed of any model-tunnel combination. At this choked condition the following effects occur: first, the restriction of the flow by the model has caused a higher effective stream velocity than indicated; second, the longitudinal pressure gradients along the flexible tunnel walls have been altered greatly; third, for all airfoils operating at lift, the ratio of the mass flow over the upper surface to that over the lower surface has been changed; and, fourth, an angle-of-attack change, necessitated by the asymmetrical characteristics of the mass flow, has been incurred. Because of the seriously altered flow conditions, the data at the choking Mach number are of questionable value and have no known significance in relation to airplane design.

At speeds between the critical and choking conditions the data are subject to variable errors in Mach number, dynamic pressure, and angle of attack. Measurements of the pressures along the Langley 24-inch high-speed tunnel walls in the plane of symmetry of the model (reference 4) were used to determine the longitudinal velocity gradient over a chord length of the test section opposite the model location. The velocity variation over this length was approximately 2 percent of the free-stream Mach number at a Mach number of 0.03 below choking condition. Limited data from the Langley rectangular high-speed tunnel, which has a slightly smaller effective tunnel height than the Langley 24-inch high-speed tunnel, are in agreement with the results of reference 4. This 2-percent gradient is not believed to affect data seriously and therefore, the effects of constriction on data at Mach numbers of more than 0.03 below choking conditions are not expected

to be of great importance. The approximate magnitude of the
constriction effect, as shown in reference 4, appears small at the
critical speed for low lift coefficients and for ratios of model
thickness to tunnel height less than 0.03.

In this paper the pressure diagrams and the data showing the
variation of normal-force and moment coefficients with Mach number
are presented for the complete attainable speed range; all cross-
plots include only data at Mach numbers up to 0.03 below choking
condition. No constriction correction has been applied to the data.
The theoretically derived corrections (reference 5), however, based
on the assumption of small induced velocities at subcritical Mach
numbers, should provide an indication of the magnitude of the tunnel-
wall effects. The following relations, determined by the method
of reference 5, are approximately correct at the subcritical speeds
for all airfoils tested:

$$\text{Corrected } M = 1.010 \times \text{Test } M$$

$$\text{Corrected } c_n = 0.96 \times \text{Test } c_n$$

$$\text{Corrected } c_{m_c/4} = 0.003 + \text{Test } c_{m_c/4}$$

Humidity.- Unpublished data from the Langley 24-inch high-speed
tunnel indicate that the aerodynamic characteristics of an airfoil
at high Mach numbers may vary with the humidity of the air at the
tunnel entrance. Humidity effects have been found to be minimized
by making all tests when the relative humidity of atmospheric air at
the tunnel entrance is below 70 percent. This procedure was followed
for the present tests; therefore, these data are not expected to be
considerably affected by atmospheric humidity.

Test section Mach number gradients.- At Mach numbers below a
value of 0.82 the longitudinal gradient varied not more than ±0.5 per-
cent of the indicated stream Mach number. Below a Mach number of 0.6,
cross-tunnel gradients over ±80 percent of the tunnel semiheight,
were about ±0.8 percent of the stream Mach number. At a stream Mach
number of 0.85 the cross-tunnel gradient increased to ±1.7 percent
of the stream Mach number.

Air-stream alinement.- Inaccuracies in alinement of the model
with the air stream can introduce a possible error of 0.2° at the 0°
setting of the model. Incremental angle changes should, however, be
within 0.1° of the angles indicated.

Tunnel-speed calibration.- Tunnel-speed calibration can be checked
to within ±0.8 percent of free-stream Mach number through the Mach

number range of 0.25 to 0.85. The effect of the model on the pressure
at the calibrated static plates is small, never exceeding 1 percent.

Velocity fluctuations.- At times short-period fluctuations of
the tunnel speed were noticed. These fluctuations were possibly
associated with a chordwise oscillating motion of the shock wave
over the surface of the model. All measurements, however, were
taken under steady conditions. The manometer used for pressure-
distribution measurements is incapable of responding to rapid pressure
fluctuations and, therefore, pressure-distribution diagrams cannot
be expected to correspond accurately to true instantaneous pressure in
the neighborhood of the shock wave.

RESULTS

The results of the pressure-distribution tests are presented in
graphical form. The basic curves are plotted as nondimensional
pressure coefficient P against percent-chord location to show the
load distribution of the normal forces. The area of this type of
curve is proportional to the normal-force coefficient c_n while the
distribution of the area determines the moment coefficient $c_{m_{c/4}}$.

The normal-force and moment coefficients presented herein have been
obtained by integration of the pressure-distribution diagrams. For
the angular range covered in these tests, no appreciable difference
exists between the normal-force coefficient and lift coefficient or
between the moment coefficient based on normal forces and the moment
coefficient based on true lift components.

Schlieren photographs have been included for visualization of
the flow phenomena. Compression shocks are indicated by approximately
straight lines, either dark or light, generally extending perpendicularly
from the surface of the airfoil model. The severity of the shock
cannot be compared between photographs because of the changes in
sensitivity of the schlieren system. Flow separation shown on these
photographs appears the same way on low-speed smoke-flow photographs.
Imperfections in the glass end plates, which appear in figures 31
and 32 as wavy lines extending from the edge of the photograph above
the upper surface toward the leading edge, should not be confused as
stream disturbances.

DISCUSSION

Pressure Distributions and Schlieren Photographs

The chordwise pressure distributions of the models are presented in figures 3 to 30. Each figure shows the effect of compressibility on the pressure distribution for a given angle of attack α. The critical-pressure coefficient, the line labeled P_{cr} on each of the higher speed pressure-distribution diagrams, denotes the pressure coefficient corresponding to the local velocity of sound.

Subcritical.- The pressure-distribution figures corresponding to subcritical speeds for the low angles of attack and small normal-force coefficients show that increases in Mach number in the subcritical range are accompanied by increases in the maximum negative pressure coefficients. These increases are in agreement with theory and previous experimental work (reference 1).

A comparison of the pressure-distribution diagrams for the conventional and low-drag types of airfoil (figs. 4 and 16) illustrates the fundamental difference between these sections. The location of the low-speed peak-pressure coefficient, and, consequently, the position of early shock formation, are considerably farther back on the low-drag model as a result of the rearward location of the maximum thickness.

Supercritical.- Compression shock in the supercritical speed range is shown on the pressure-distribution diagrams by the comparatively rapid compression which occurs at some location rearward of the location of the low-speed maximum negative-pressure coefficient. The location of this region of discontinuity moves rearward with increasing Mach number. A better understanding of the supercritical pressure diagrams can be had by comparing figure 4 with the schlieren photographs of figure 31 which show the general case of shock movement over a surface. The consolidation of the shock disturbances on the lower surface from the incipient condition at a Mach number of 0.742 (fig. 31(b)) to a single well-defined shock disturbance at a Mach number of 0.769 (fig. 31(c)) is also shown. Dissymmetry of flow over the upper and lower surfaces as a result of attitude is evident in figures 32 and 7; this dissymmetry is indicated in figure 31 to a lesser degree as a result of camber. These data agree with the results of reference 1. Such movements of shock waves over the surface near the trailing edge, and the subsequent pressure changes, suggest large changes in control-surface characteristics.

The supercritical flow photographs (figs. 31 to 33) show that flow separation occurs from the surface having the higher induced velocity and that separation from both surfaces is possible. The location of the separation point also appears to be generally upstream of the most rearward part of the shock formation at the high supercritical Mach numbers. The vast majority of schlieren photographs of various type airfoils taken in the Langley rectangular high-speed tunnel are in agreement with these observations. High-speed schlieren movies of the air flow over models in the Langley rectangular high-speed tunnel at constant-stream Mach number have shown that rapid oscillations of the shock wave, separation point, and separated wake also occur for many airfoils at some supercritical speed range (reference 6). Flow separation or these oscillations could seriously alter the characteristics of the main flow and would tend to reduce any chordwise-pressure gradients which may be present in flows at supercritical speeds.

Effects of Mach Number on Wake

Figure 34 shows the variation of the location of the wake center behind the NACA 23015 airfoil with normal-force coefficient using Mach number and angle of attack as parameters. The intersection of the chord line of the model at $0°$ angle of attack with the survey plane 0.5 chord downstream of the trailing edge fixes the reference line. The location of the center of wake (location of maximum total-pressure loss) below this reference line determines the wake center location shown in figure 34. The change in the location of the wake center in these two-dimensional tests is considered an indication of possible flow direction change.

Subcritical.- A decrease in wake-center displacement for any constant positive normal-force coefficient is seen to occur as Mach number is increased. Most of the indicated difference between the curves at subcritical speeds is the direct result of changing the angle of attack as the reference line remained fixed; therefore, no change in down-flow angle at constant angle of attack is inferred. Theoretical studies (reference 7) indicate that the field of influence of the model in the subcritical speed range increased with Mach number at the same rate as given for the lift coefficient in reference 8. At a constant angle of attack, therefore, compressibility should have little or no effect on the angle of down flow at subcritical speeds.

Supercritical.- At supercritical speeds there is a definite indication that large changes in downflow may be expected. In figures 3, 33, and 34, as well as 4, 31, and 34, are presented comparative data for low-lift conditions of the NACA 23015 airfoil. Shock location as determined by the schlieren photographs is comparable with

that shown on the pressure-distribution diagrams. Only small
differences in flow conditions for the upper and lower surfaces
can be noticed from the photographs. The wake-center location at
low lift coefficients at any Mach number, consequently, does not
vary appreciably from that at low speeds. On the other hand, at
high lift conditions, pressure distributions (fig. 7) indicate and
the schlieren photographs (fig. 32) reveal a large separated region
over the upper surface which results in a large change in wake-center
location with Mach number (fig. 34). In this speed range, therefore,
the unsymmetrical nature of the accompanying violent separation of
flow appears to be the factor which controls the wake-center location.
These data indicate that the present theoretical estimations of down-
wash are probably inaccurate at supercritical speeds as a result of
separation. These data also indicate the possibility of radical
changes in airplane longitudinal trim characteristics at supercritical
speeds.

Prediction of Pressure Coefficients

For comparative purposes the experimental variation with Mach
number of the peak negative pressure coefficient is plotted on
figure 35 with the pressure-coefficient variation predicted by two
theoretical methods (references 8 and 9). The value of pressure
coefficients used in this figure are the maximum negative pressure
coefficients attained over a surface without regard of chordwise
location.

The Glauert approximation, reference 8, is the simplest
correction to apply. The approximation worked out by Kaplan,
reference 9, is more exact than that by Glauert and is of approxi-
mately the same magnitude as that obtained by von Kármán from the
hodograph method (reference 10). As a general rule, the Glauert
approximation tends to underestimate the changes, and it appears
from figure 35 that better results for an average value of the peak
negative-pressure coefficient could be obtained by use of Kaplan's
approximation.

Critical Mach Number

Since the critical Mach number is a criterion for determining
the speed at which changes in the character of the flow are to be
expected, the critical Mach number is of great importance in the
selection of a wing section. For high-speed operation at low drag
coefficient the critical speed of an airfoil section, or any body,
should not be exceeded.

The variation of the critical Mach number with normal-force coefficient is presented for each airfoil in figure 36. It is evident that, regardless of thickness, the NACA 23015 airfoil has a lower critical speed than any of the other airfoils. The forward location of maximum thickness and camber on this airfoil produce high pressure peaks at relatively low lifts and, therefore, lower critical speeds are to be expected. Both the NACA 23015 and the NACA 65(216)-418 sections have a very large range of normal-force coefficient where the critical Mach number is slowly decreasing.

Three effects of an increase in camber are illustrated by a comparison of the curves of the NACA 66,2-015 and NACA 66,2-215 airfoils: a decrease of the critical Mach number which is in agreement with the results of reference 11; a shift of the range of high critical Mach number to higher normal-force coefficients; and, a slight increase in the normal-force coefficient range for high critical Mach number. The latter effect is probably caused by a reduction of the pressure peak at high Mach number on the leading edge for the cambered section (figs. 18 and 22). These results indicate that the effects of compressibility should be carefully considered in determining the camber of a wing for high-speed aircraft.

Normal Force

The variation with Mach number of the normal-force coefficient for each airfoil at all angles of attack tested is presented in figures 37 to 41. The critical Mach number M_{cr} for each angle is indicated by the dashed curve.

A general increase in the slope of these curves (figs. 37 to 41) with increasing Mach number or angle of attack is apparent in the Mach number range below the peak normal-force coefficient. At subcritical speeds, this increase in slope with Mach number for each of the airfoils tested follows the general trend predicted by theory (see fig. 37 and reference 8) and shown by experiment (references 1, 2, and 3). At supercritical speeds the development and rearward motion of the compression shock over one surface, while the velocities over the opposite surface are still subsonic (see fig. 13) tend to cause the increase in slope with Mach number. The rapid decrease in the normal forces at the highest Mach numbers (figs. 37 to 41) probably results from two causes: first, flow separation from the upper surface which has been aggravated by the influence of the shock wave; and, second, the more rapidly increasing negative pressures corresponding to local supersonic velocities near the trailing edge on the lower surface where the flow is less inclined to separate. (Curves for data within 0.03 of choking Mach number are dotted on these figures.)

An increase in the angle of attack generally increases the absolute pressure difference between the upper and lower surfaces, moves the location of the maximum negative pressures rearward over the lower surface and forward over the upper surface, and decreases the critical speed of the upper surface (figs. 3 to 30). The result of these changes is an increase in the slope of the curves at the higher angles of attack (figs. 37 to 41) in the speed range below the region of decreasing normal-force coefficients.

Normal-force coefficient data are plotted against angle of attack on figures 42 to 46. The slopes $\dfrac{\partial c_n}{\partial \alpha}$ of these curves continue to increase up to that Mach number where the normal forces of figures 37 to 41 decrease rapidly; this behavior is expected from the preceding discussion. The variation in normal-force curve slope with Mach number for the airfoils investigated is summarized in figure 47. A comparison of the slopes for the conventional and low-drag-type airfoils shows no marked differences. The NACA 23015 airfoil and the NACA 16-212 airfoil have more gradual variations of normal-force curve slope with Mach number than the other airfoils; this fact indicates that these airfoils should produce less change in airplane longitudinal trim as a result of lift changes. The NACA 16-series airfoil, however, has a low normal-force curve slope; tests in the Langley 8-foot high-speed tunnel have also indicated a low lift-curve slope of the NACA 16-212 airfoil.

The normal-force-coefficient data for the NACA 23015 airfoil at the higher angles of attack, figure 37, do not increase as expected. At supercritical velocities violent separation occurs well forward on the chord and restricts any decrease in pressure over the rear portion of the upper surface. The magnitude of the negative pressure peak near the leading edge which produces a large portion of the normal force at low speeds is also decreased considerably with increasing Mach number.

Delay of normal-force break.- The increment ΔM between the critical Mach number and the Mach number at which a rapid change in the normal-force characteristic (force break) originates M_{l_b} is presented in figure 48. At low angles of attack a Mach number increment from 0.03 to 0.04 is shown for all the newer airfoils; the conventional NACA 23015 airfoil exhibits a Mach number increment of about 0.13 at these low angles. As the angle of attack is increased to approximately 4°, however, the Mach number increment for the newer models of 0.15 thickness ratio or less rapidly approaches the value for the conventional airfoil which has remained almost constant. At an angle of attack of 4° pressure distributions at subcritical speeds for the newer airfoils

(figs. 12, 18, and 22) approach the general shape of the pressure distributions for the NACA 23015 airfoil (figs. 4 to 6); that is, the maximum pressure coefficient is located well forward at low speeds and a considerable rearward latitude of shock motion is thereby allowed. As the critical speed is exceeded and the shock wave moves rearward, pressures corresponding to supersonic speeds are thus maintained over an increasingly large part of the upper surface. A considerable Mach number range with relatively regular variation of lift is then possible.

At an angle of attack of 6° for the NACA 23015 airfoil the flow has been changed by pronounced separation and oblique shock waves (fig. 32); the pressure distribution (fig. 7) and the delay of the force break (fig. 48) are therefore affected. An angle of attack of 4° was not sufficient to change the basic shape of the pressure distribution for the thicker NACA 65(216)-418 airfoil (fig. 29); at 6°, however, the familar peak due to angle of attack is evident (fig. 30) and a considerably increased delay of the force break (fig. 48) is apparent. From a consideration of these data, the increment between the critical and the Mach number for normal-force break therefore appears closely related to the location of the maximum negative pressure coefficient.

Although conclusions concerning the optimum profile of an airfoil cannot be drawn from these data, it is indicated that estimates of airfoil section characteristics at supercritical speeds based on the critical Mach number must be qualified somewhat when working with sections of various types. In order to obtain desirable control characteristics at speeds in excess of the highest critical Mach number possible by the use of any practicable airfoil, it may be advisable to select that airfoil having the normal-force break at the highest Mach number possible even though its critical Mach number may be somewhat lower than that of other sections.

Shift of zero lift angle.- For the NACA 16-212 airfoil (fig. 38) all normal-force curves in the higher Mach number range, including those at negative angles of attack, tend to slope in a negative direction. The pressure-distribution diagrams for the NACA 16-212 airfoil at angles of attack from -4° to 0° (figs. 8, 9, and 10) show that the negative loading near the leading edge increases rapidly with Mach number. The resulting drop in normal force with Mach number for all angular configurations indicates an increase in the angle of attack for zero lift as the Mach number is increased. This angular shift or decrease in the effective camber of the section (which can contribute to catastrophic diving tendencies) is clearly illustrated for several airfoils in figures 43, 44, and 46. This angular shift can be caused by one or both of the following factors, increased flow separation or the decreased

influence of the model on the approaching flow as the Mach number
is increased. Flow separation directly affects the pressures over
the rear of the model; also as the Mach number is increased to
values approaching and beyond the critical, the pressure impulses
from the various parts of the body encounter increased difficulty in
progressing upstream from their origins. As a result of these effects,
the oncoming air is not affected as far ahead of the model or as
greatly at these speeds as at low speeds and the whole character of
the flow field is transformed.

The NACA 23015 airfoil (fig. 42) is the only cambered airfoil
tested which does not present this angular shift. Inspection of
the pressure-distribution diagrams for this model (figs. 3 and 4)
reveals a marked similarity of the pressure distribution over the
upper and lower surfaces near zero lift; therefore, an appreciable
shift in the angle of zero lift is not expected.

Quarter-Chord Moment

The basic data for the moment coefficient, obtained by intergration
of the normal-force pressure-distribution diagrams, are presented in
figures 49 to 53. The arrows indicate the critical Mach number for
each angle of attack. A comparison of these figures indicates com-
paratively low values of moment coefficient for both the
NACA 23015 airfoil, and the NACA 66,2-015 airfoil.

From the results of reference 11 for a thickness ratio of 0.15, a
negative shift of 0.05 in moment coefficient occurs at medium speeds
for a camber increase of approximately 1 percent. The difference in
moment coefficients for the NACA 66,2-015 and the NACA 66,2-215 airfoils
(for which a camber difference of slightly over 1 percent exists) is
indicated at low angles of attack by figures 51 and 52 to be in good
agreement with the results of reference 11.

The variation of moment coefficient with normal-force coefficient
is shown in figures 42 to 46. The rates of change of the moment and
normal-force coefficients with angle of attack are plotted against
Mach number on figures 47 and 54. Data from figures 47 and 54 were
combined to show the rate of change of moment coefficient with normal-
force coefficient $\frac{\partial c_{m_{c/4}}}{\partial c_n}$ at several Mach numbers. Points calculated
by this method, as well as the actual slopes of the curves on figures 42
to 46, were used to determine the curves on figure 55. The slopes of

the moment curves $\dfrac{\partial c_{m_{c/4}}}{\partial c_n}$ or $\dfrac{\partial c_{m_{c/4}}}{\partial \alpha}$ should not become more negative

at high Mach numbers. A positive trend of the slope of the moment
curve (fig. 55) (corresponding to a decrease in stability), is
desired since airplanes have exhibited greatly increased stability
at high speeds (reference 12). All of the newer airfoils tested had

a positive trend of $\dfrac{\partial c_{m_{c/4}}}{\partial c_n}$ at the higher Mach numbers; the con-

ventional NACA 23015 airfoil had a negative trend.

CONCLUSIONS

The results of the tests of the five airfoils considered herein
have shown that:

1. For constant moderate normal-force coefficients, pronounced
separation of the flow occurred from only one surface of the
NACA 23015 airfoil at supercritical speeds. This separation produced
large variations with Mach number of the location of the center of
the wake.

2. The camber of the wing section should be carefully selected
to insure high values of the critical speed of the wing section at
any design condition.

3. The Mach number increment between the critical speed and the
Mach number of the normal-force break, which affects control character-
istics at supercritical speeds, appears to be closely related to the
location of the low-speed maximum negative-pressure coefficient. At
low angles of attack, this increment was approximately 0.13 for the
NACA 23015 airfoil and approximately 0.03 for the newer type airfoil
sections.

4. A shift in the angle of zero lift occurred at high Mach numbers
for all the newer cambered airfoils tested. This shift was attributed
to flow separation and to the decreased influence of any disturbance
on the oncoming stream.

5. Since airplanes have exhibited greatly increased stability
at high speeds, the positive trend for the change of pitching moment

coefficient with normal-force coefficient found for all the newer
airfoils tested with increasing Mach number is desirable; the trend
for the NACA 23015 airfoil with increasing Mach number was negative.

Langley Memorial Aeronautical Laboratory
    National Advisory Committee for Aeronautics
        Langley Field, Va.

REFERENCES

1. Stack, John, Lindsey, W. F., and Littel, Robert E.: The
   Compressibility Burble and the Effect of Compressibility on
   Pressures and Forces Acting on an Airfoil. NACA Rep. No. 646,
   1938.

2. Stack, John: The N.A.C.A. High-Speed Wind Tunnel and Tests of
   Six Propeller Sections. NACA Rep. No. 463, 1933.

3. Stack, John, and von Doenhoff, Albert E.: Tests of 16 Related
   Airfoils at High Speeds. NACA Rep. No. 492, 1934.

4. Byrne, Robert W.: Experimental Constriction Effects in High-Speed
   Wind Tunnels. NACA ACR No. L4L07a, 1944.

5. Allen, H. Julian, and Vincenti, Walter G.: Wall Interference in
   a Two-Dimensional-Flow Wind Tunnel with Consideration of the
   Effect of Compressibility. NACA ARR No. 4K03, 1944.

6. Daley, Bernard N., and Humphreys, Milton D.: Effects of
   Compressibility on the Flow past Thick Airfoil Sections.
   NACA RM No. L6J17a, 1947

7. Prandtl, L: General Considerations on the Flow of Compressible
   Fluids. NACA TM No. 805, 1936.

8. Glauert, H: The Effect of Compressibility on the Lift of an
   Aerofoil. R. & M. No. 1135, British A.C.R., 1927.

9. Kaplan, Carl: The Flow of a Compressible Fluid past a Curved
   Surface. NACA ARR No. 3K02, 1943.

10. von Kármán, Th.: Compressibility Effects in Aerodynamics. Jour.
    Aero. Sci., vol. 8, no. 9, July 1941, pp. 337-356.

11. Stack, John: Tests of Airfoils Designed to Delay the Compressibility
    Burble. NACA TN No. 976, Dec. 1944. (Reprint of ACR, June 1939.)

12. Bielat, Ralph P.: Effect of Compressibility on Longitudinal Stability
    and Control of $\frac{1}{5.5}$-Scale Model of Fighter Airplane. NACA ACR
    No. L4J02, 1944.

CONFIDENTIAL

TABLE I.- ORDINATES OF AIRFOILS

[Stations and ordinates in percent of wing chord]

NACA 23015

Station	Upper surface	Lower surface
0	- - -	0
1.25	3.34	-1.54
2.50	4.44	-2.25
5.00	5.89	-3.04
7.50	6.90	-3.61
10.00	7.64	-4.09
15.00	8.52	-4.84
20.00	8.92	-5.41
25.00	9.08	-5.78
30.00	9.05	-5.96
40.00	8.59	-5.92
50.00	7.74	-5.50
60.00	6.61	-4.81
70.00	5.25	-3.91
80.00	3.73	-2.83
90.00	2.04	-1.59
95.00	1.12	-.90
100.00	.16	-.16

L.E. radius: 2.48. Slope of of radius through L.E. 0.305

NACA 16-212

Upper surface		Lower surface	
Station	Ordinate	Station	Ordinate
0	0	0	0
.241	.672	.359	-.608
.527	.957	.673	-.839
1.160	1.396	1.340	-1.182
2.395	1.988	2.605	-1.616
4.883	2.822	5.117	-2.190
7.379	3.454	7.621	-2.606
9.879	3.972	10.121	-2.938
14.886	4.804	15.114	-3.458
19.897	5.459	20.103	-3.867
24.911	5.979	25.089	-4.189
29.927	6.389	30.073	-4.445
34.944	6.703	35.056	-4.643
39.962	6.926	40.038	-4.784
44.981	7.059	45.019	-4.869
50.000	7.103	50.000	-4.897
55.019	7.056	54.981	-4.866
60.038	6.906	59.962	-4.764
65.055	6.639	64.945	-4.579
70.071	6.241	69.929	-4.297
75.084	5.698	74.916	-3.908
80.093	4.994	79.907	-3.402
85.095	4.113	84.905	-2.767
90.088	3.032	89.912	-1.998
92.082	2.541	91.918	-1.653
94.072	2.010	93.928	-1.288
95.066	1.729	94.934	-1.097
96.059	1.437	95.941	-.903
98.041	.816	97.959	-.504
100.000	.120	100.000	-.120

L.E. radius: 0.703. Slope of radius through L.E.: 0.084

NACA 66,2-215

Upper surface		Lower surface	
Station	Ordinate	Station	Ordinate
0	0	0	0
.407	1.156	.593	-1.056
.647	1.395	.853	-1.255
1.136	1.748	1.364	-1.534
2.370	2.411	2.630	-2.039
4.856	3.399	5.144	-2.767
7.350	4.178	7.650	-3.330
9.848	4.851	10.152	-3.817
14.855	5.926	15.145	-4.580
19.868	6.759	20.132	-5.167
24.886	7.410	25.114	-5.620
29.906	7.904	30.094	-5.960
34.929	8.260	35.071	-6.200
39.952	8.486	40.048	-6.344
44.976	8.590	45.024	-6.400
50.000	8.563	50.000	-6.357
55.023	8.389	54.977	-6.199
60.045	8.032	59.955	-5.890
65.063	7.435	64.937	-5.375
70.076	6.568	69.924	-4.624
75.081	5.546	74.919	-3.756
80.080	4.411	79.920	-2.819
85.070	3.217	84.930	-1.871
90.052	2.004	89.948	-.970
95.026	.875	94.974	-.243
100.000	0	100.000	0

L.E. radius: 1.384. Slope of radius through L.E.: 0.084
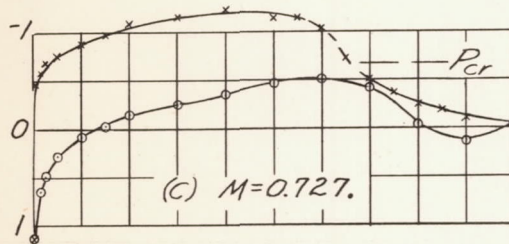
CONFIDENTIAL

NATIONAL ADVISORY
COMMITTEE FOR AERONAUTICS

CONFIDENTIAL

TABLE I.- ORDINATES OF AIRFOILS - Concluded

[Stations and ordinates in percent of wing chord]

NACA 66,2-015	
Station	Upper or lower surface ordinate
0	0
.500	1.110
.750	1.329
1.250	1.645
2.500	2.229
5.000	3.086
7.500	3.757
10.000	4.337
15.000	5.255
20.000	5.964
25.000	6.516
30.000	6.933
35.000	7.230
40.000	7.415
45.000	7.495
50.000	7.460
55.000	7.294
60.000	6.961
65.000	6.405
70.000	5.597
75.000	4.652
80.000	3.616
85.000	2.545
90.000	1.488
95.000	.560
100.000	0
L.E. radius: 1.384	

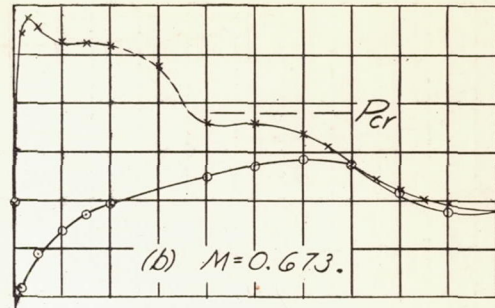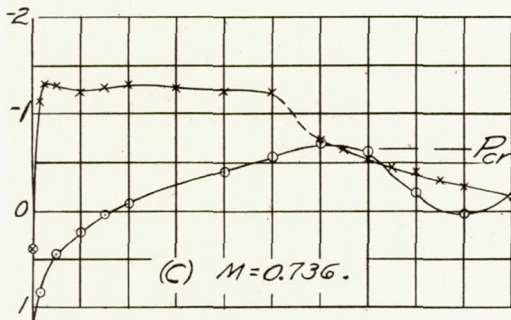| NACA 65(216) 418			
Upper surface		Lower surface	
Station	Ordinate	Station	Ordinate
0	0	0	0
.275	1.433	.725	-1.233
.504	1.722	.996	-1.442
.972	2.216	1.528	-1.788
2.173	3.173	2.827	-2.429
4.628	4.601	5.372	-3.337
7.113	5.689	7.887	-3.993
9.611	6.593	10.389	-4.525
14.630	8.039	15.370	-5.347
19.668	9.124	20.332	-5.940
24.715	9.944	25.285	-6.364
29.768	10.542	30.232	-6.654
34.825	10.937	35.175	-6.817
39.884	11.135	40.116	-6.851
44.943	11.120	45.057	-6.740
50.000	10.837	50.000	-6.425
55.052	10.272	54.948	-5.892
60.094	9.448	59.906	-5.164
65.125	8.412	64.875	-4.292
70.143	7.244	69.857	-3.356
75.147	5.992	74.853	-2.412
80.137	4.693	79.863	-1.509
85.113	3.387	84.887	-.695
90.077	2.136	89.923	-.068
95.036	1.013	94.964	+.250
100.000	0	100.000	0
L.E. radius: 1.960. Slope of radius through L.E.: 0.168			

CONFIDENTIAL

NATIONAL ADVISORY
COMMITTEE FOR AERONAUTICS

Fig. 1   NACA RM No. L6L16

CONFIDENTIAL

INDUCTION NOZZLE ——————

FIXED WALL —————

END PLATES AND MODEL—

PARALLEL LIGHT ————

COLLIMATING LENS ————

LIGHT SOURCE —————

HIGH-PRESSURE AIR

FLEXIBLE WALL

CONDENSING LENS

CAMERA

KNIFE EDGE

WALL-ADJUSTING SCREWS

SCREENS OVER TUNNEL ENTRANCE

AIR FLOW

NATIONAL ADVISORY
COMMITTEE FOR AERONAUTICS
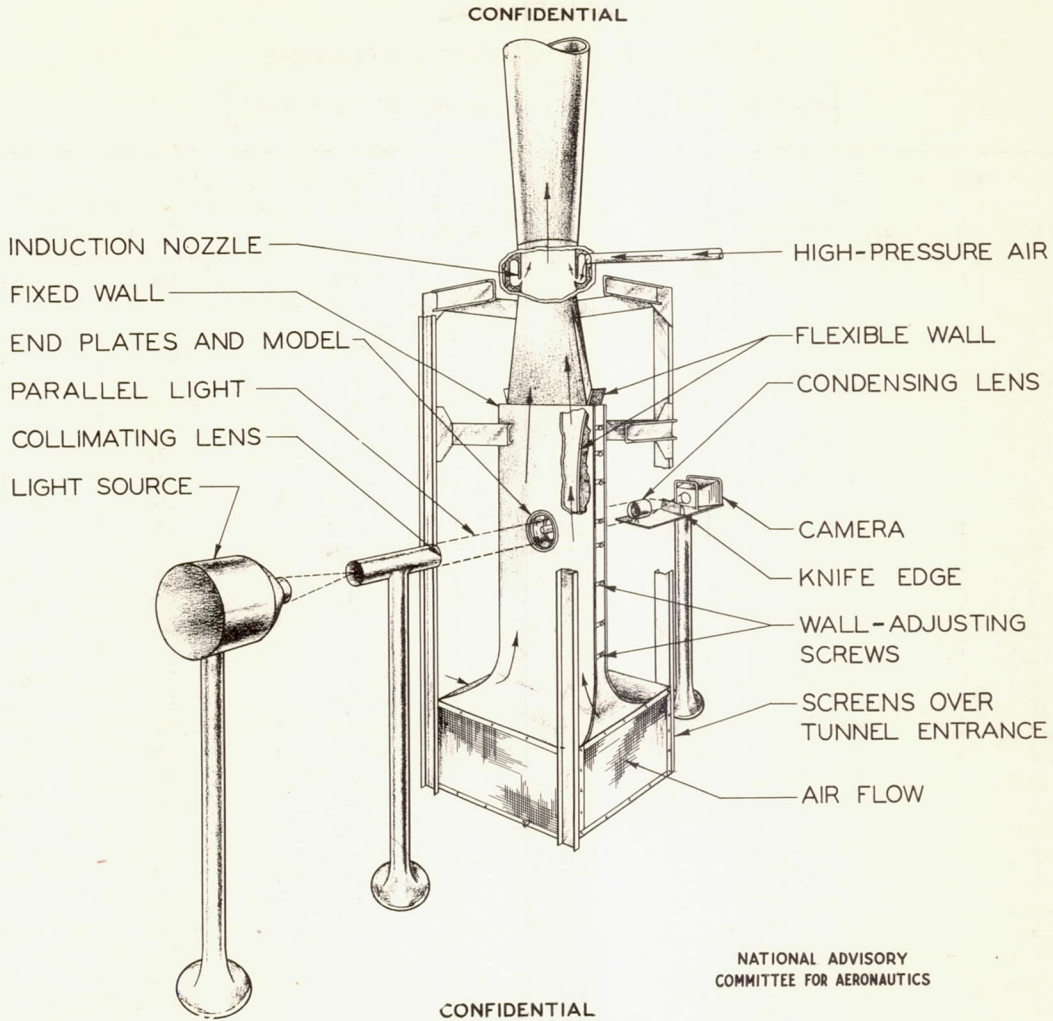
CONFIDENTIAL

FIGURE I.— SCHEMATIC DIAGRAM OF THE LANGLEY RECTANGULAR
HIGH-SPEED TUNNEL AND OPTICAL EQUIPMENT.

CONFIDENTIAL

NACA 65(216)-41<u>8</u>

NACA 66,2-015

NACA 66,2-215

NACA 23015

NACA 16-212
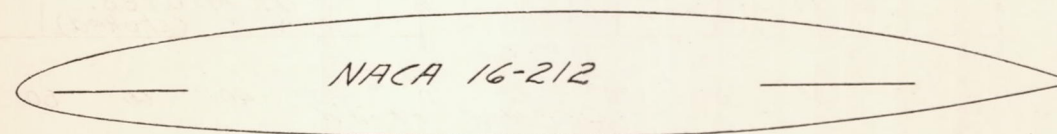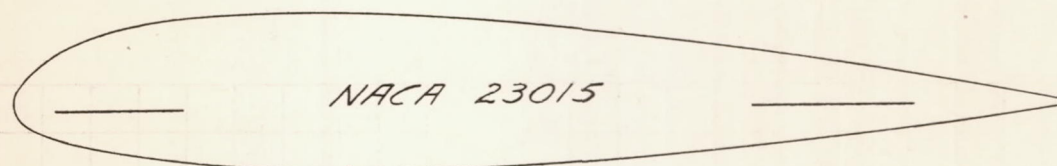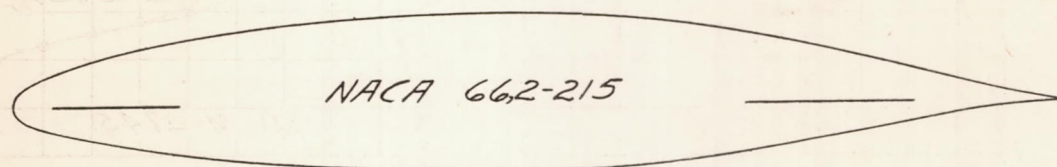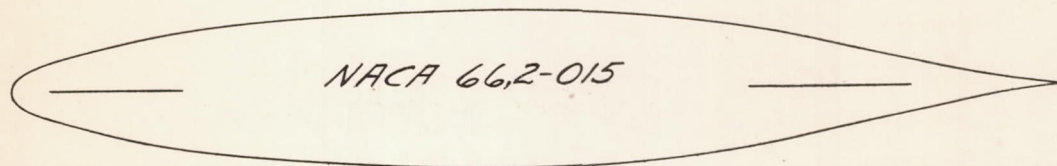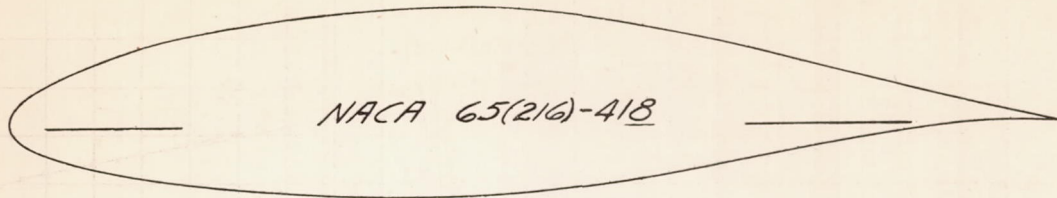
CONFIDENTIAL

NATIONAL ADVISORY
COMMITTEE FOR AERONAUTICS

Figure 2 .- Profiles of airfoils tested in the Langley
rectangular high-speed tunnel.
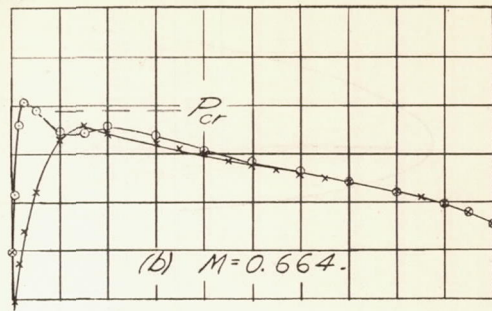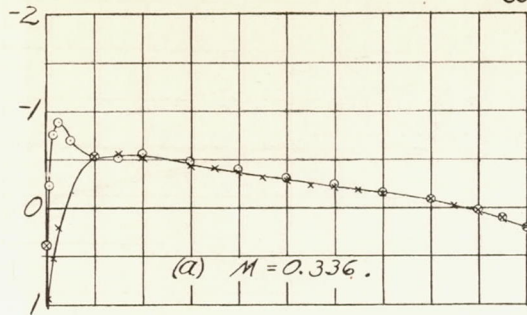
Fig. 3   NACA RM No. L6L16

CONFIDENTIAL

× Upper surface
○ Lower surface

(a) M = 0.336.

(b) M = 0.664.

(c) M = 0.716.

(d) M = 0.745.

(e) M = 0.774.

(f) M = 0.788.
(choked)

Pressure coefficient, P
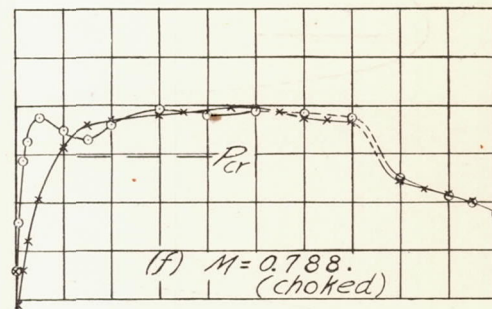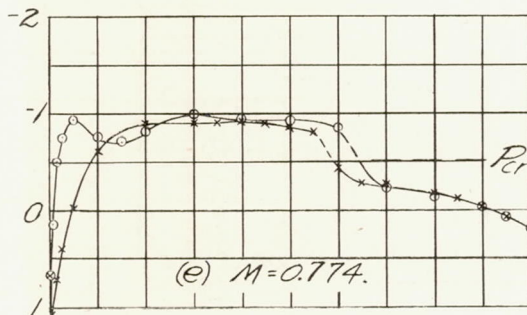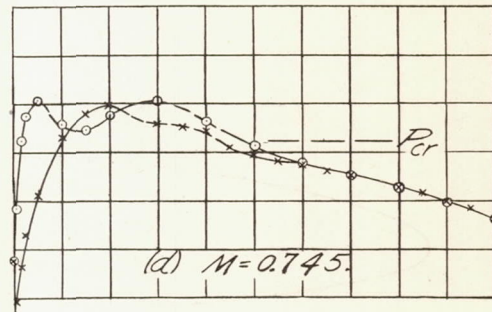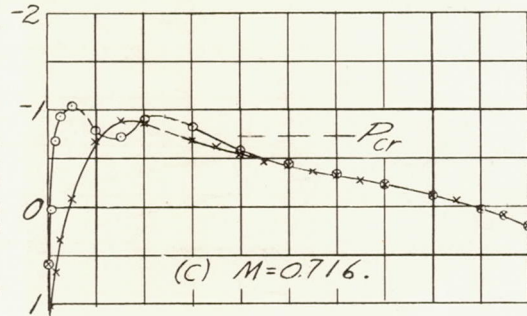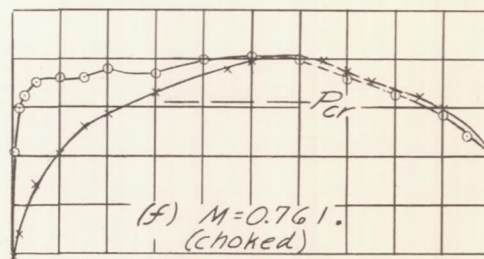
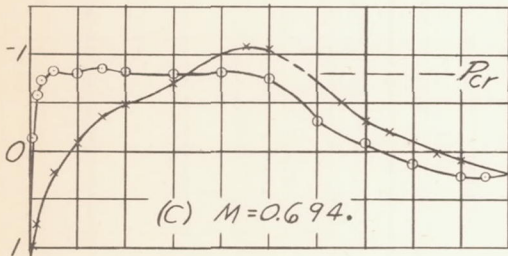Percent chord

CONFIDENTIAL

NATIONAL ADVISORY
COMMITTEE FOR AERONAUTICS

Figure 3.- Pressure distribution for the
NACA 23015 airfoil. α = -2°.

CONFIDENTIAL

×   Upper surface
⊙   Lower surface

(a) M = 0.341.

(b) M = 0.661.

(c) M = 0.715.

(d) M = 0.741.

(e) M = 0.769.

(f) M = 0.786.
(choked)

Percent chord

CONFIDENTIAL

NATIONAL ADVISORY
COMMITTEE FOR AERONAUTICS

Figure 4.— Pressure distribution for the
NACA 23015 airfoil. α = 0°.

Fig. 5   NACA RM No. L6L16
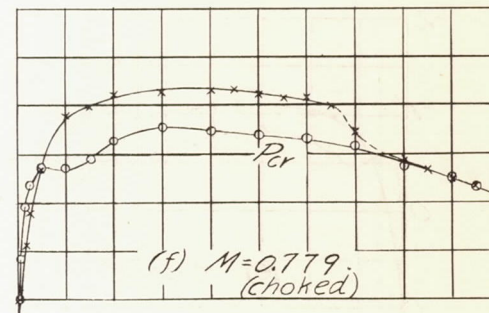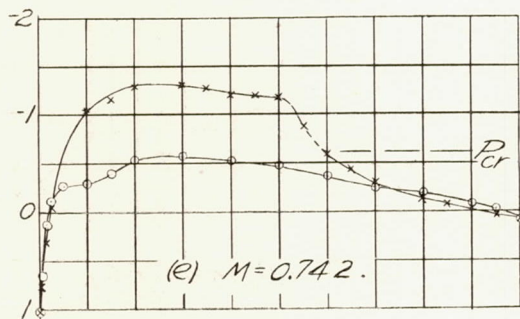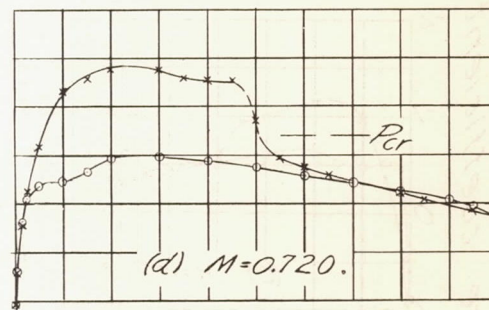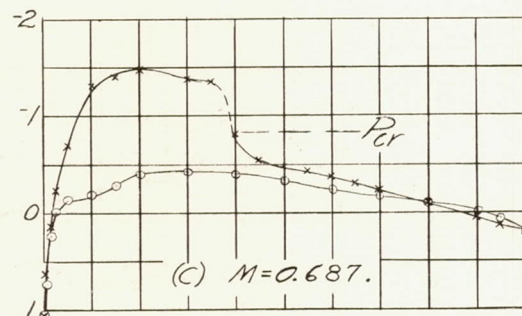
CONFIDENTIAL

Figure 5.— Pressure distribution for the
NACA 23015 airfoil.   α = 2°.
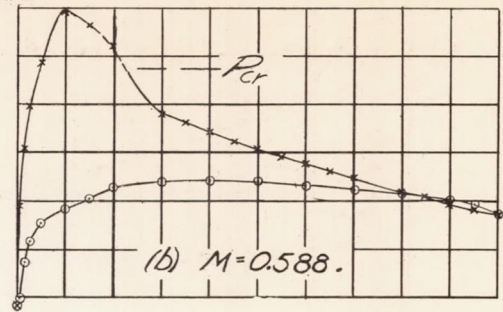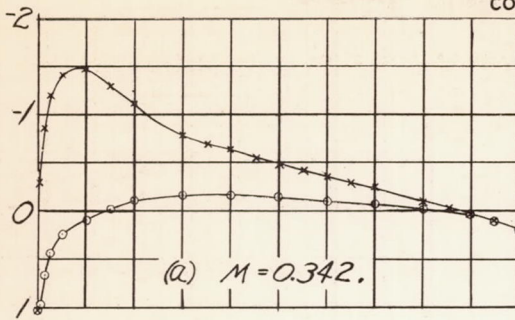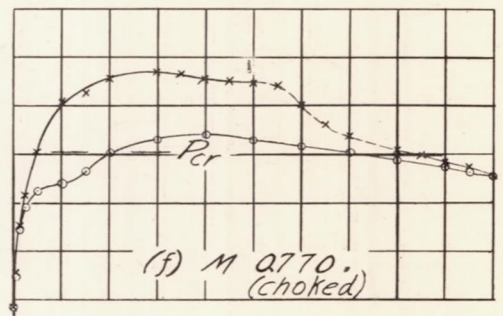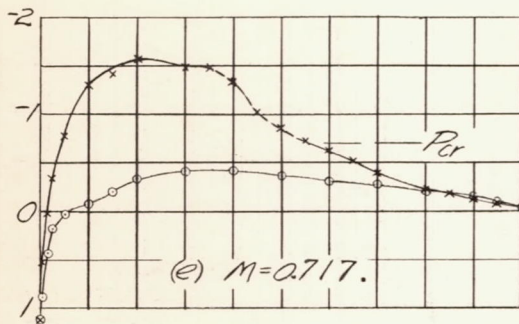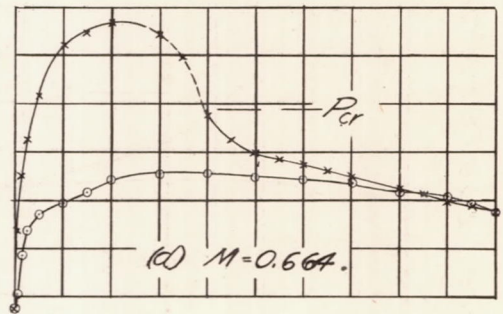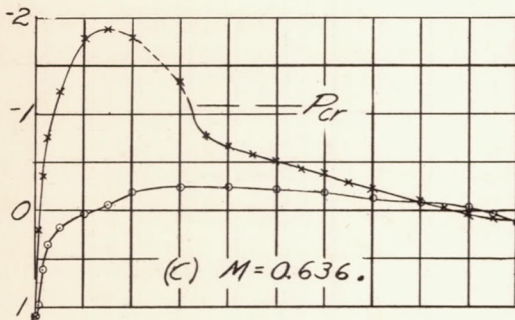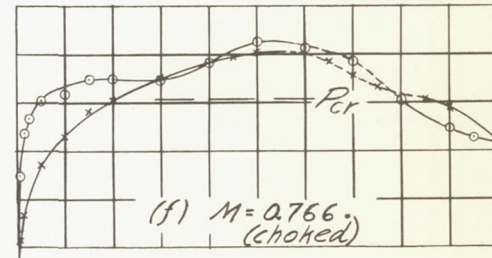
Figure 6.— Pressure distribution for the
NACA 23015 airfoil. α = 4°.

Fig. 7   NACA RM No. L6L16

CONFIDENTIAL

(a) M = 0.329.

(b) M = 0.584.

× Upper surface
⊙ Lower surface

Pressure coefficient, P

(c) M = 0.636.

(d) M = 0.690.

(e) M = 0.730.

(f) M = 0.747.
(choked at wake
survey rake)

Percent chord

CONFIDENTIAL

NATIONAL ADVISORY
COMMITTEE FOR AERONAUTICS

Figure 7.— Pressure distribution for the
NACA 23015 airfoil. $\alpha = 6°$.

CONFIDENTIAL

× Upper surface
⊙ Lower surface

(a) M=0.327.

(b) M=0.720.

P_{cr}

(c) M=0.770.

P_{cr}

(d) M=0.794.
(choked)

P_{cr}

Pressure coefficient, P

Percent chord

CONFIDENTIAL

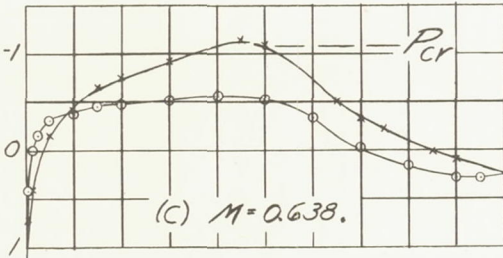NATIONAL ADVISORY
COMMITTEE FOR AERONAUTICS
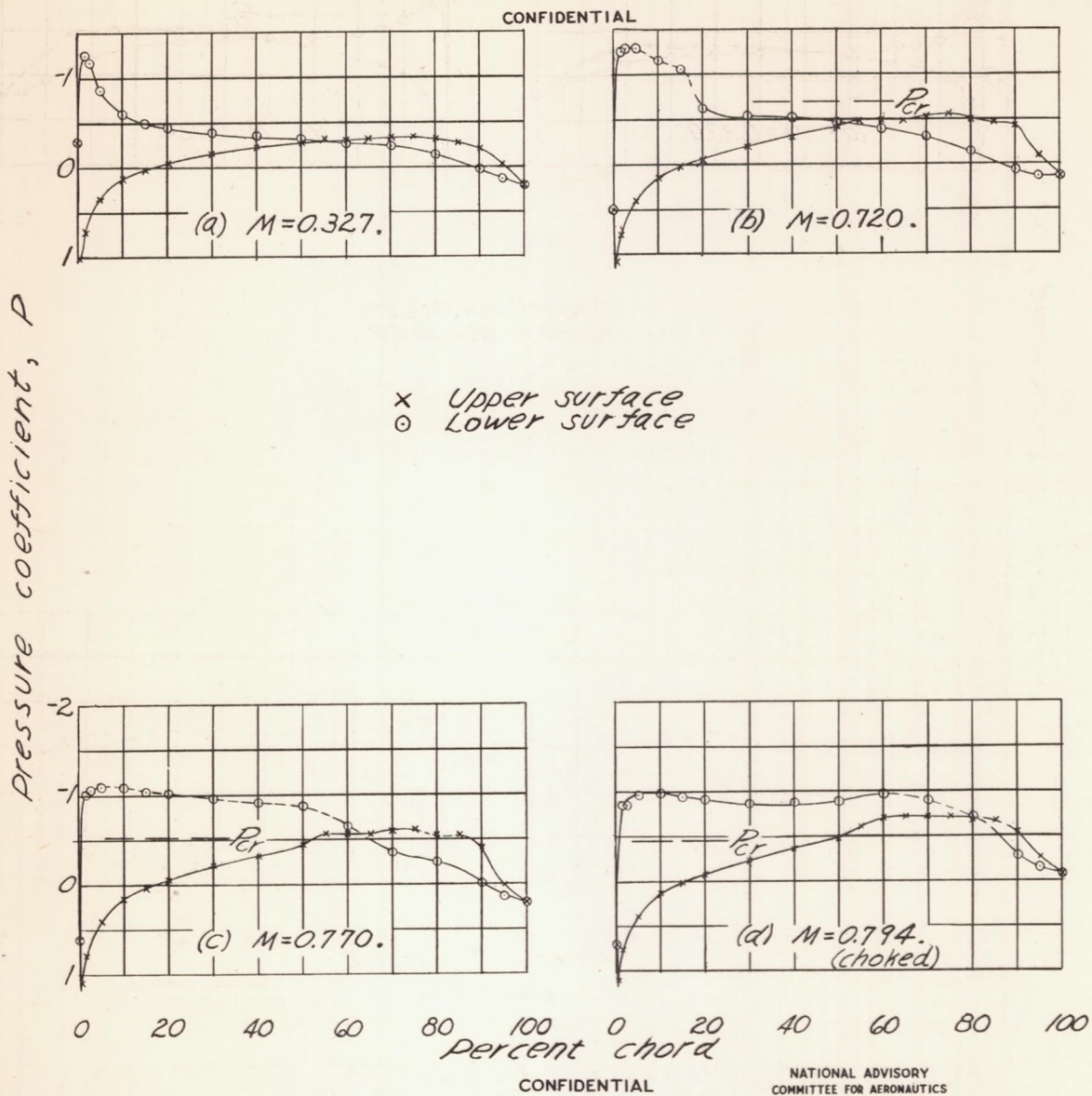
Figure 8.— Pressure distribution for the
NACA 16-212 airfoil.   α=-4°.

Fig. 9   NACA RM No. L6L16

CONFIDENTIAL

(a) M=0.329.

(b) M=0.724.

×   Upper surface
o   Lower surface

(c) M=0.779.

(d) M=0.807.
(choked)

Percent chord

CONFIDENTIAL

NATIONAL ADVISORY
COMMITTEE FOR AERONAUTICS
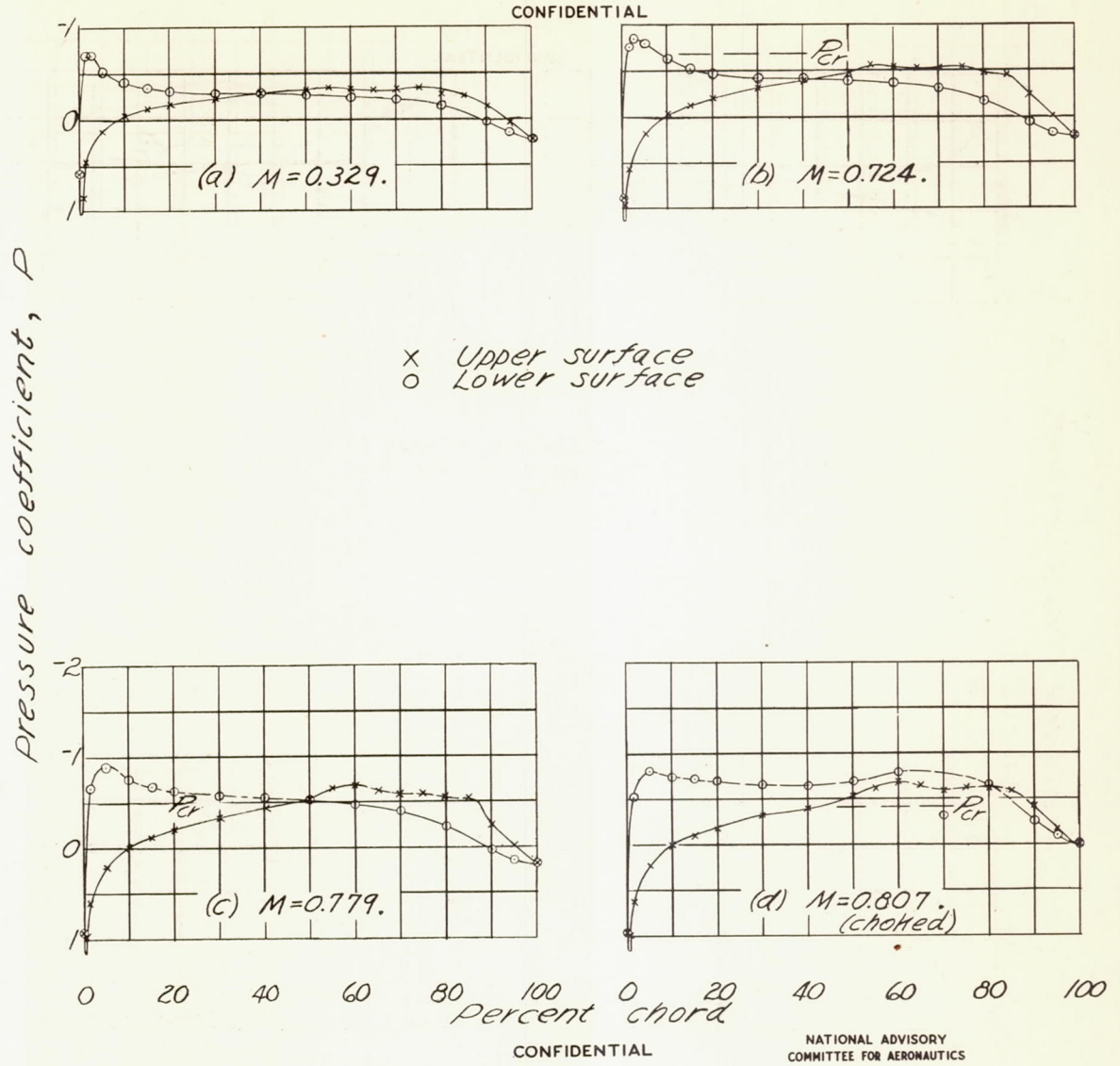
Figure 9.— Pressure distribution for the
NACA 16-212 airfoil. α=-2°.

CONFIDENTIAL

X   Upper surface
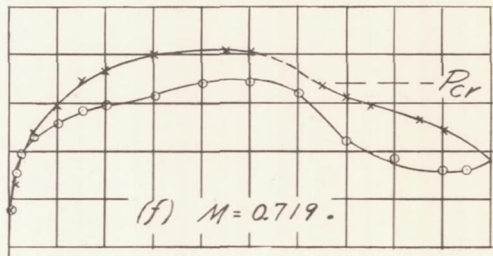O   Lower surface

CONFIDENTIAL

NATIONAL ADVISORY
COMMITTEE FOR AERONAUTICS
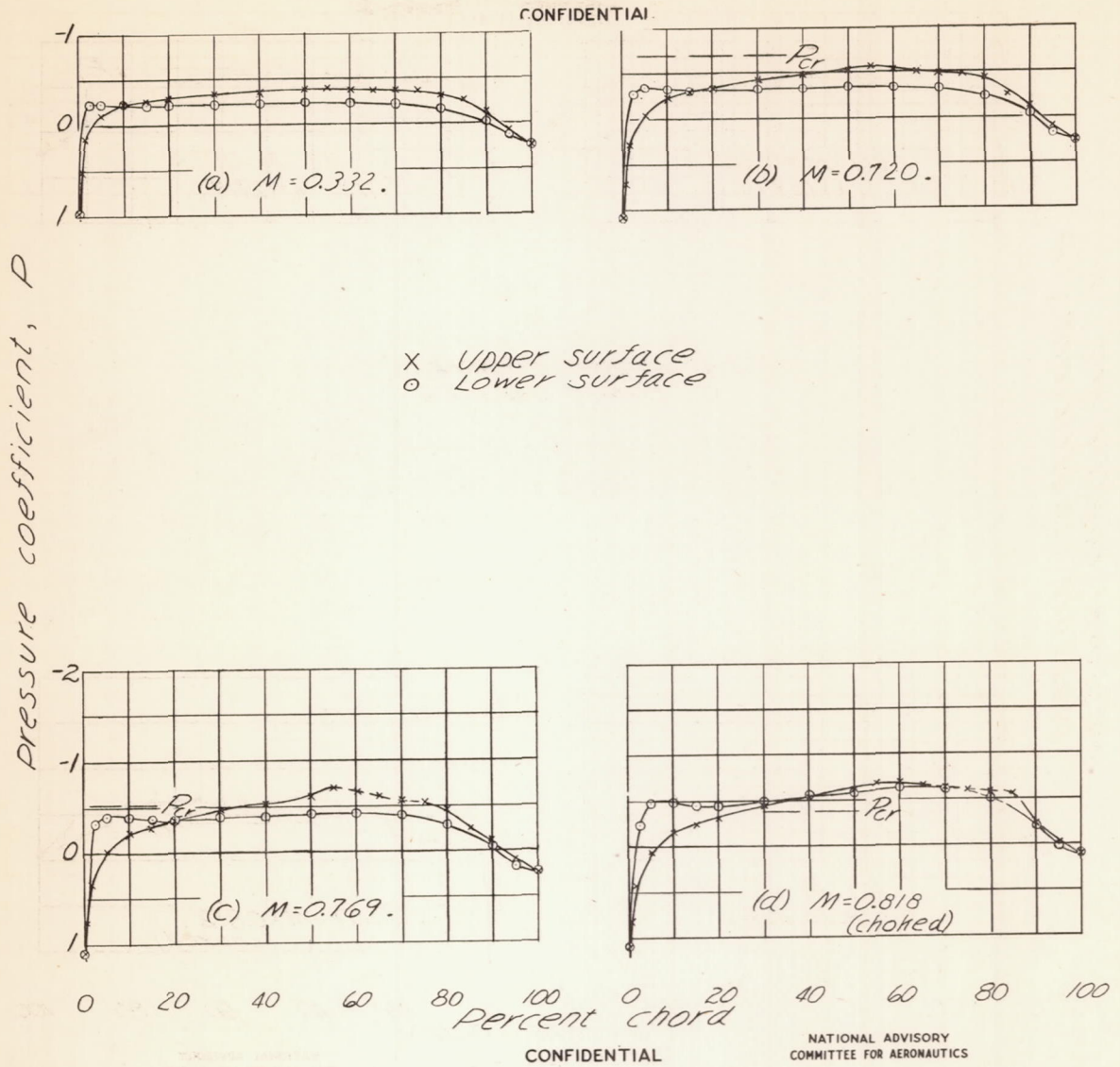
Figure 10.- Pressure distribution for the
NACA 16-212 airfoil.   α = 0°.
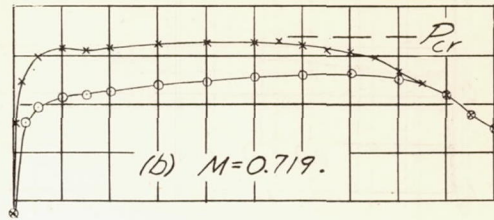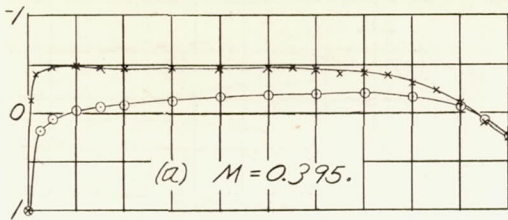
Fig. 11   NACA RM No. L6L16

CONFIDENTIAL

X   Upper surface
O   Lower surface

(a) M = 0.395.   (b) M = 0.719.
(c) M = 0.762.   (d) M = 0.812. (choked)

Pressure coefficient, P
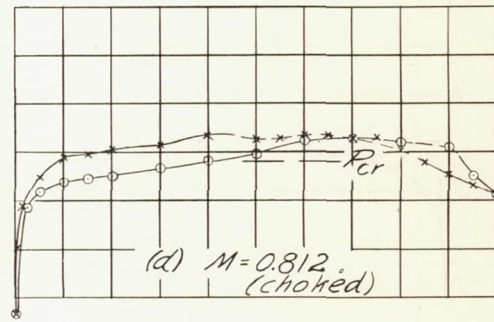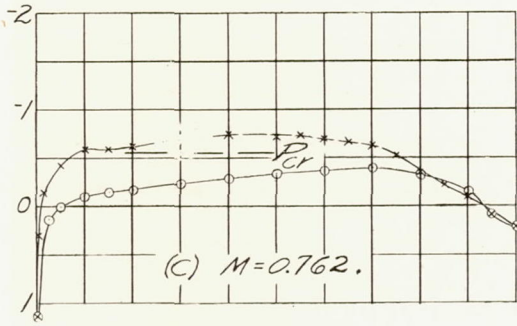
Percent chord

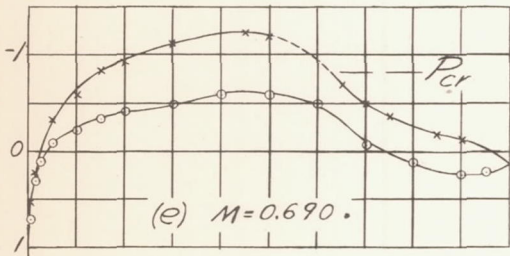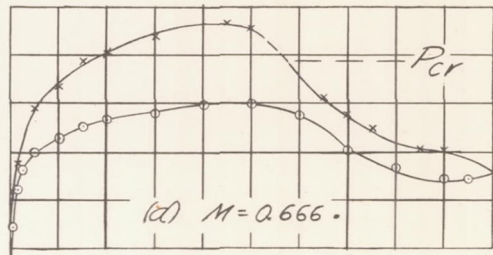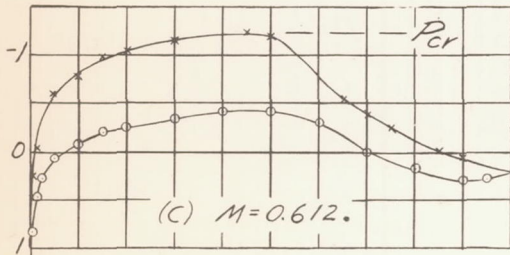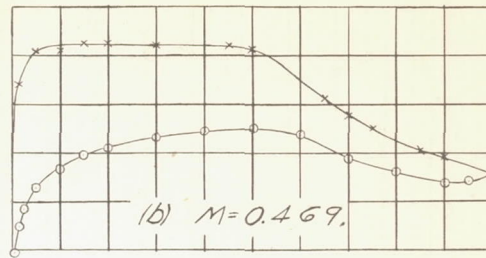CONFIDENTIAL

NATIONAL ADVISORY
COMMITTEE FOR AERONAUTICS

Figure 11.- Pressure distribution for the
NACA 16-212 airfoil. $\alpha = 2°$.
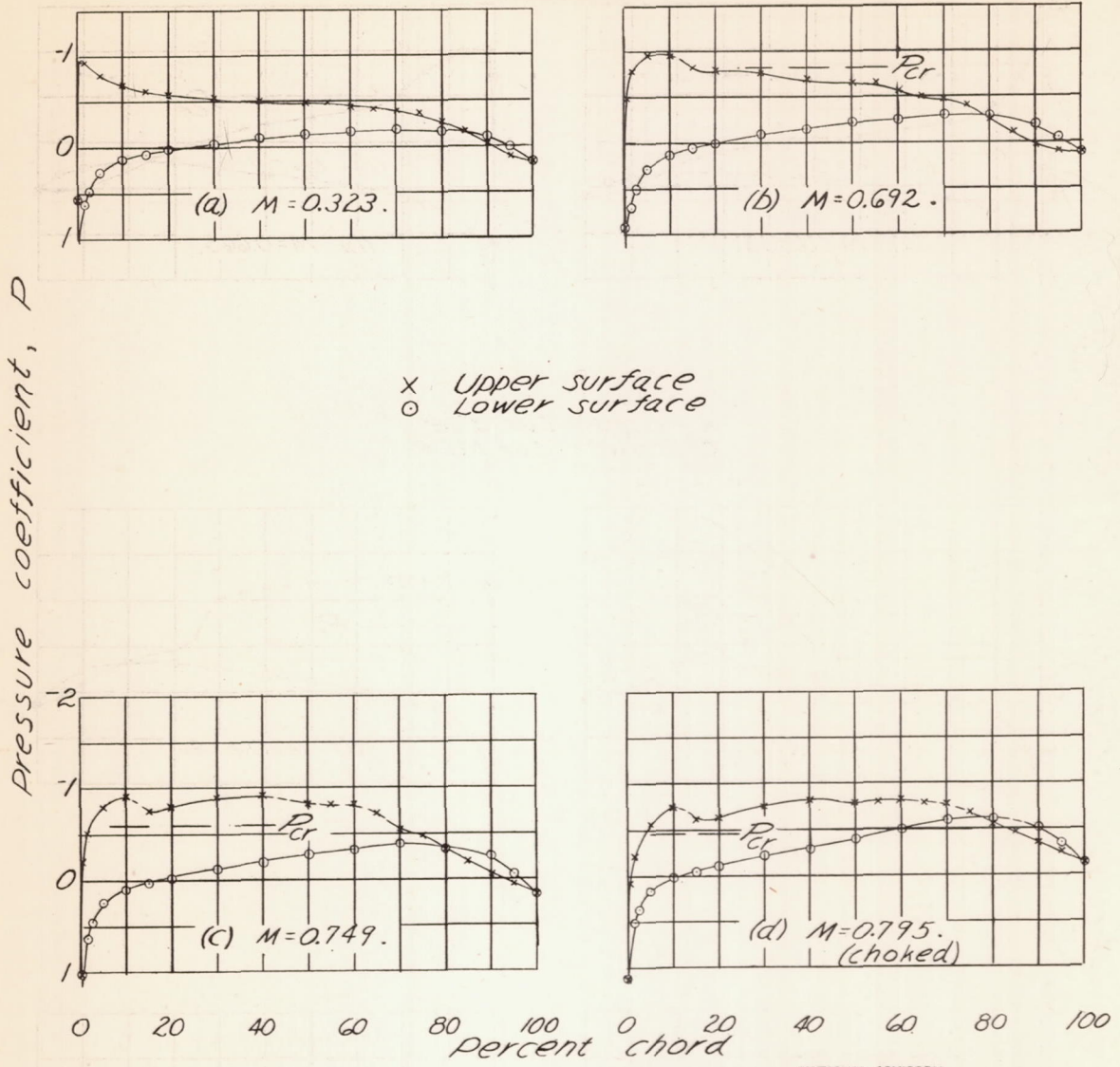
Figure 12.- Pressure distribution for the NACA 16-212 airfoil. $\alpha = 4°$.
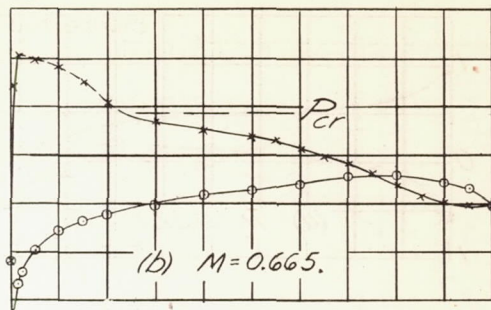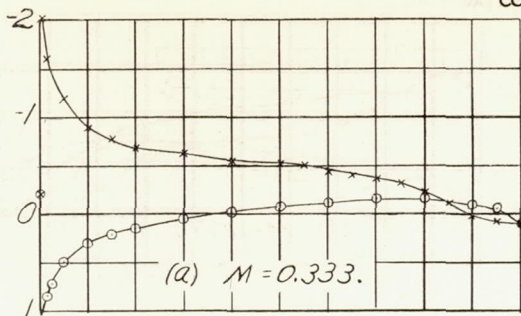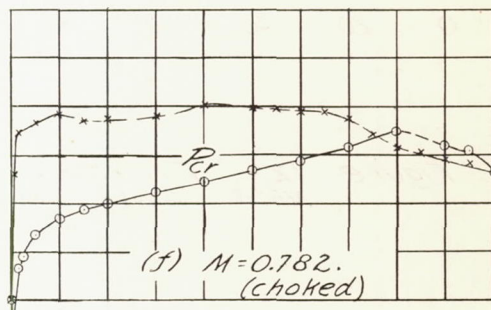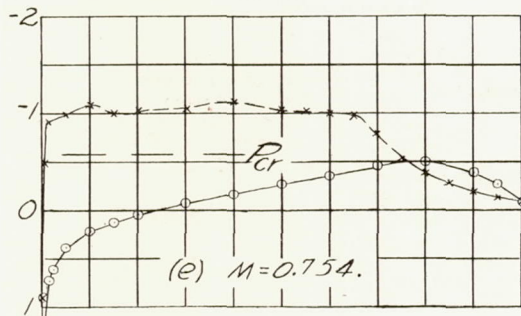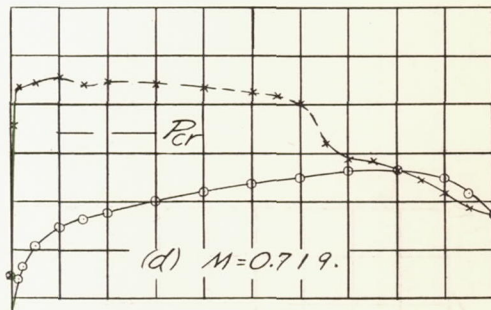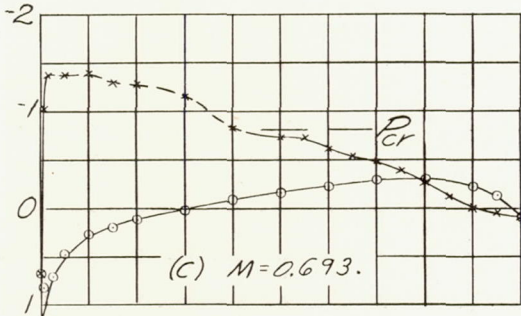
NATIONAL ADVISORY
COMMITTEE FOR AERONAUTICS

Fig. 13   NACA RM No. L6L16

CONFIDENTIAL

(a) M = 0.333.

(b) M = 0.665.

x   Upper surface
o   Lower surface

(c) M = 0.693.

(d) M = 0.719.

(e) M = 0.754.

(f) M = 0.782.
(choked)

Pressure coefficient, P

Percent chord
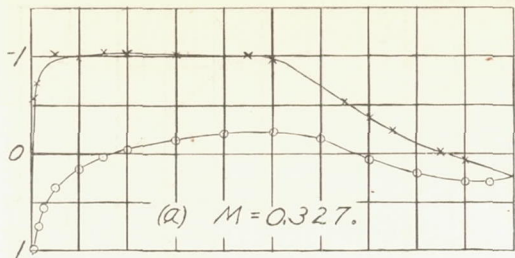
CONFIDENTIAL

NATIONAL ADVISORY
COMMITTEE FOR AERONAUTICS

Figure 13.- Pressure distribution for the
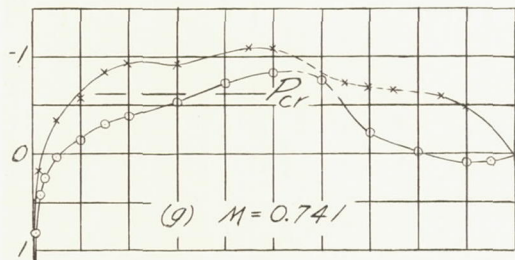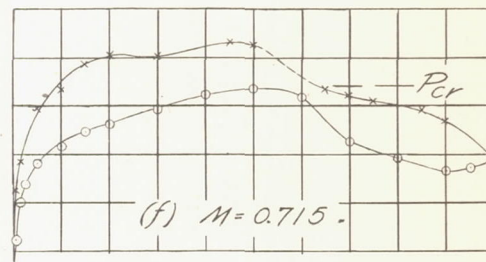NACA 16-212 airfoil. $\alpha = 6°$.

CONFIDENTIAL

Pressure coefficient, P

(a) M = 0.332.

(b) M = 0.700.

P_{cr}

×   Upper surface
⊙   Lower surface

(c) M = 0.765.

P_{cr}

(d) M = 0.780.
     (choked)

P_{cr}

Percent chord

CONFIDENTIAL

NATIONAL ADVISORY
COMMITTEE FOR AERONAUTICS
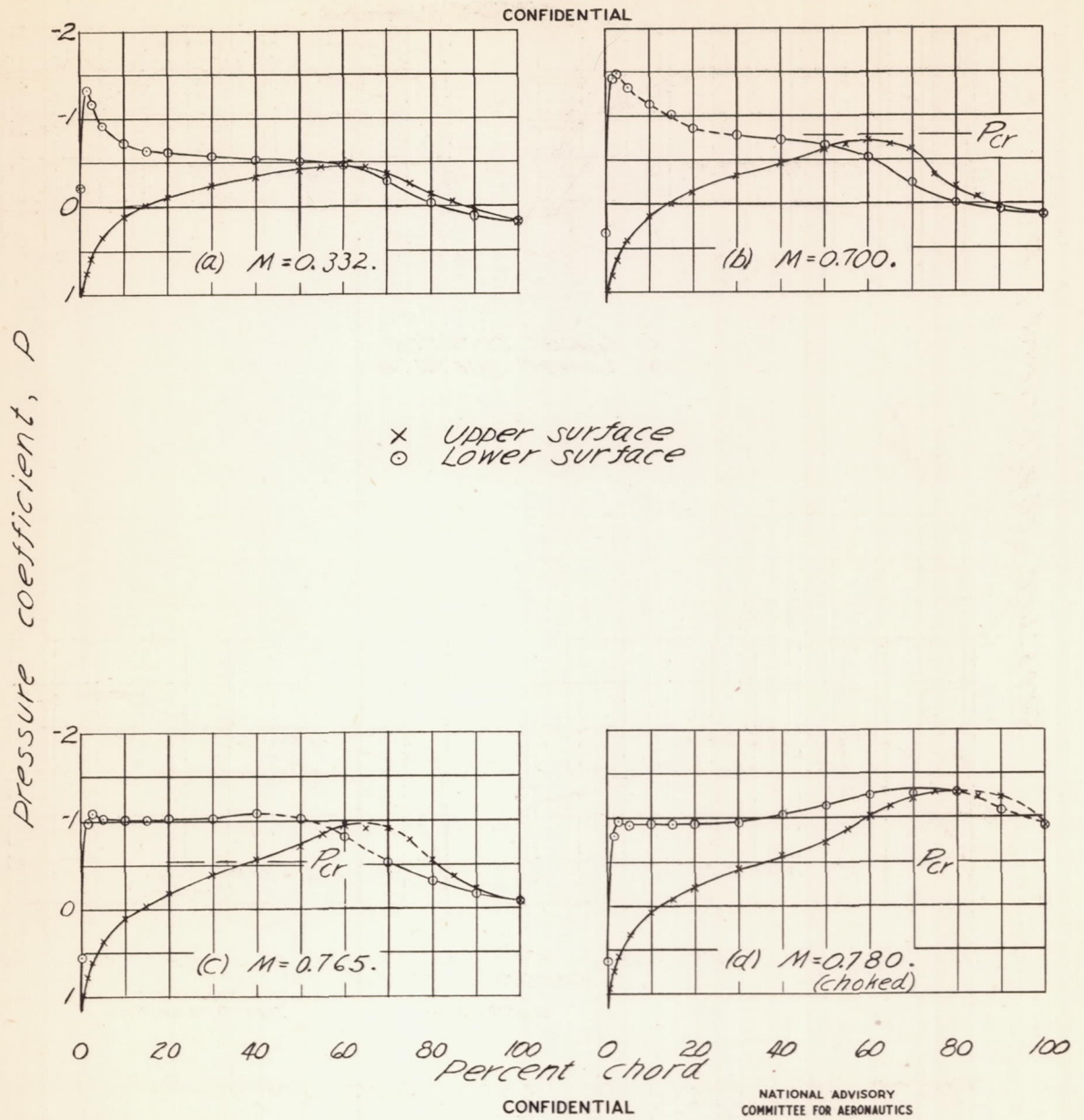
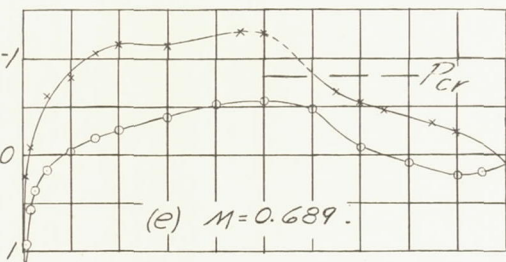Figure 14. — Pressure distribution for the
NACA 66,2-215 airfoil. $\alpha = -4°$.
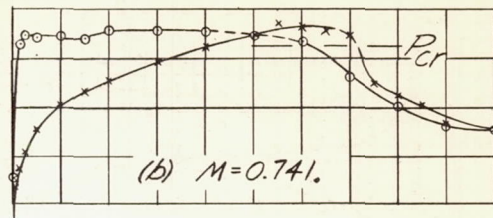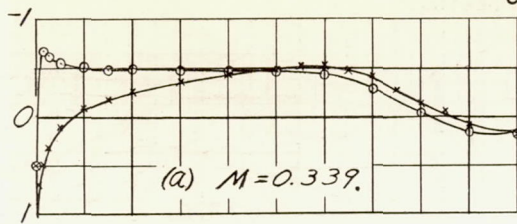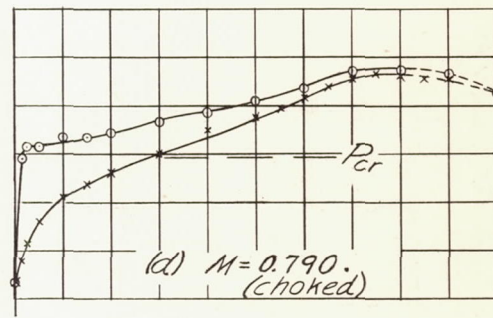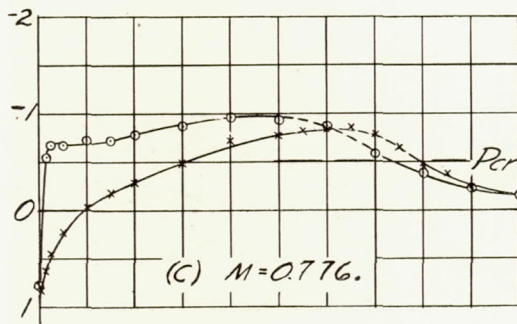
Fig. 15   NACA RM No. L6L16

CONFIDENTIAL

(a) M = 0.339.

(b) M = 0.741.

x   Upper surface
⊙   Lower surface

Pressure coefficient, P

(c) M = 0.776.

(d) M = 0.790.
(choked)

Percent chord

CONFIDENTIAL

NATIONAL ADVISORY
COMMITTEE FOR AERONAUTICS

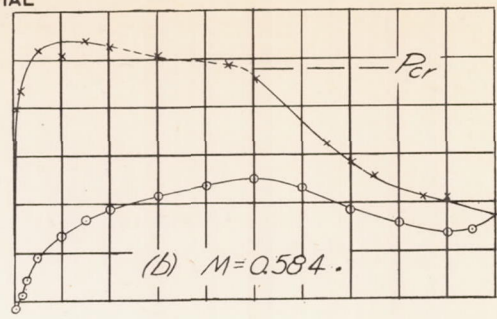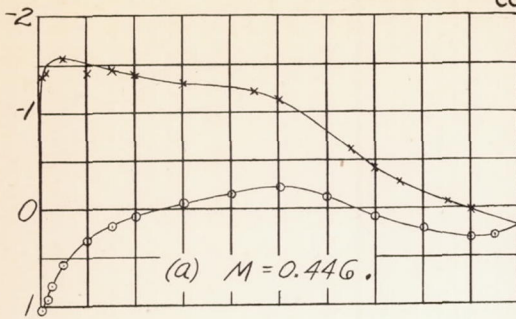Figure 15.— Pressure distribution for the
NACA 66,2-215 airfoil.   α = -2°.

CONFIDENTIAL

× Upper surface
⊙ Lower surface

Percent chord

NATIONAL ADVISORY
COMMITTEE FOR AERONAUTICS
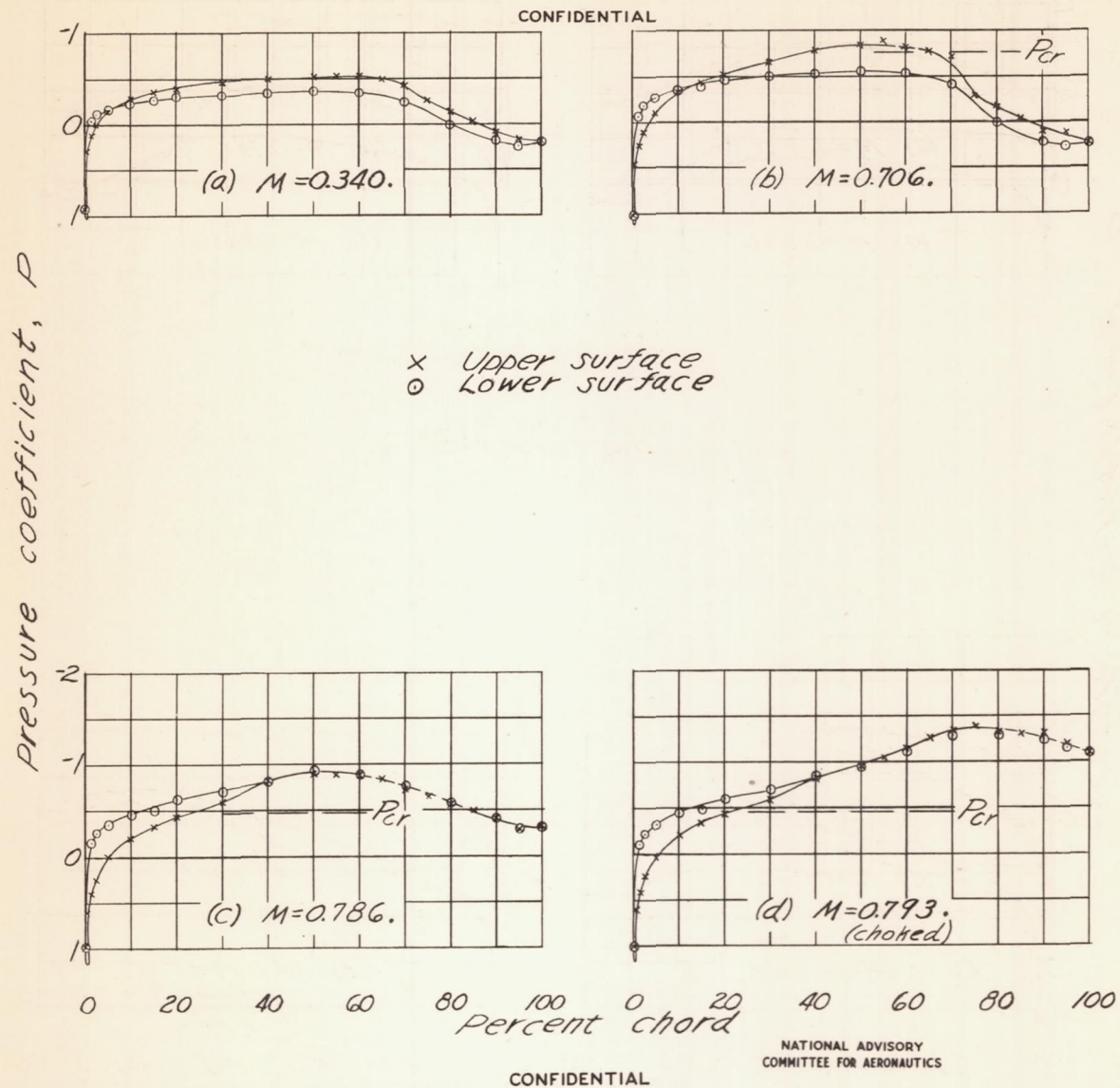
CONFIDENTIAL

Figure 16.— Pressure distribution for the
NACA 66,2-215 airfoil. α= 0°.
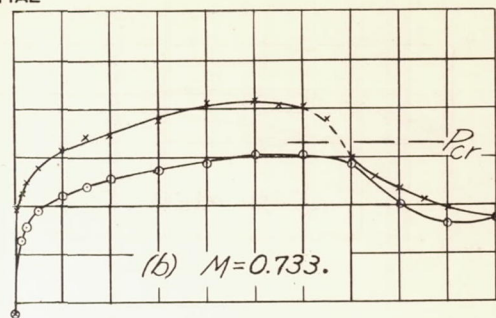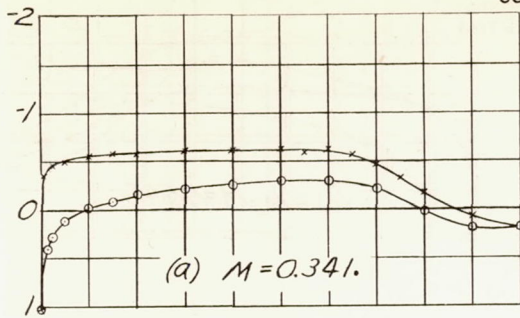
Fig. 17   NACA RM No. L6L16

CONFIDENTIAL

x   Upper surface
⊙   Lower surface

(a) M = 0.341.

(b) M = 0.733.

P_{cr}

(c) M = 0.785.

P_{cr}

(d) M = 0.794.
(choked)
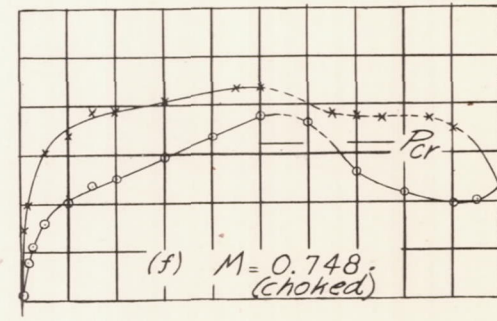
P_{cr}
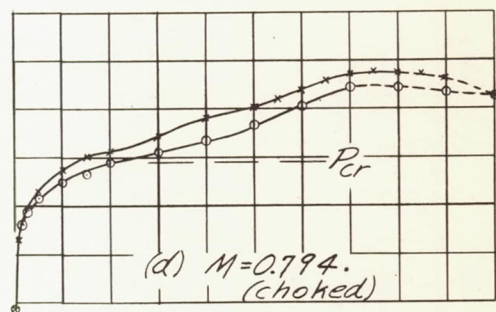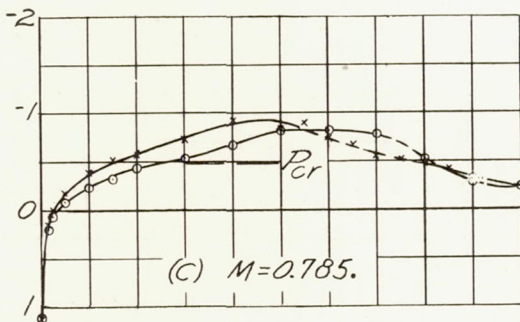
Pressure coefficient, P

Percent chord

CONFIDENTIAL

Figure 17.— Pressure distribution for the
NACA 66,2-215 airfoil. $\alpha = 2°$.

CONFIDENTIAL
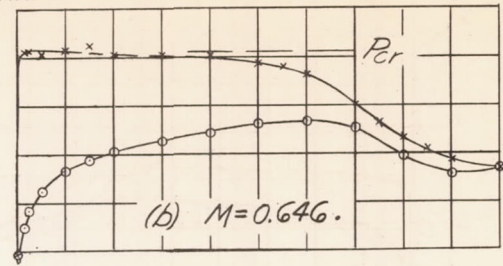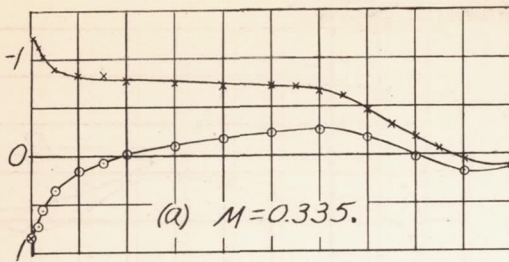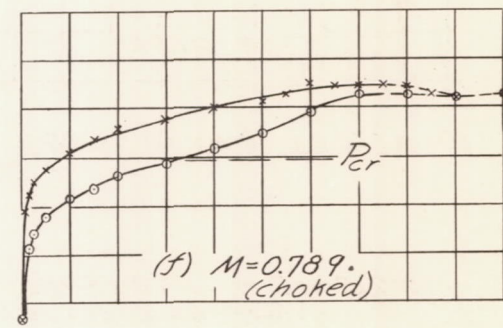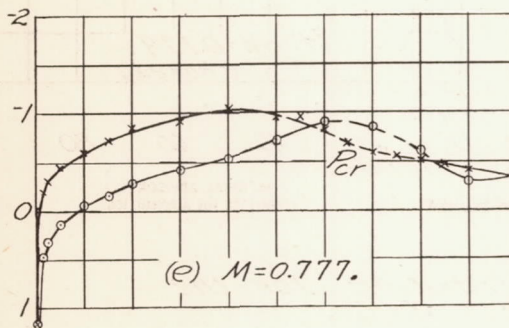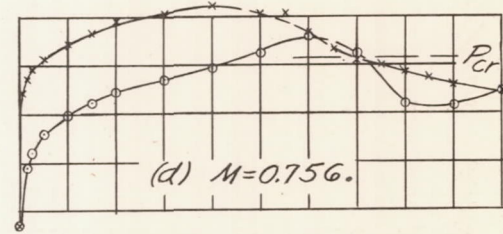
X   Upper surface
⊙   Lower surface

(a) M=0.335.

(b) M=0.646.

(c) M=0.727.

(d) M=0.756.

(e) M=0.777.

(f) M=0.789.
(choked)

Pressure coefficient, P

Percent chord
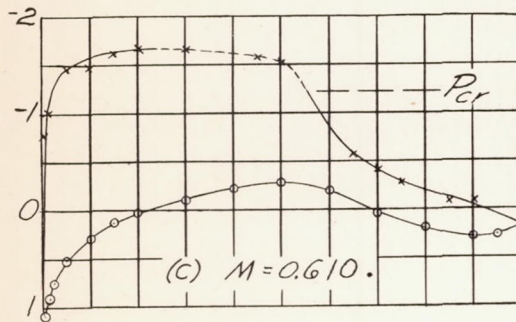
CONFIDENTIAL

NATIONAL ADVISORY
COMMITTEE FOR AERONAUTICS

Figure 18.- Pressure distribution for the
NACA 66,2-215 airfoil.   α=4°.
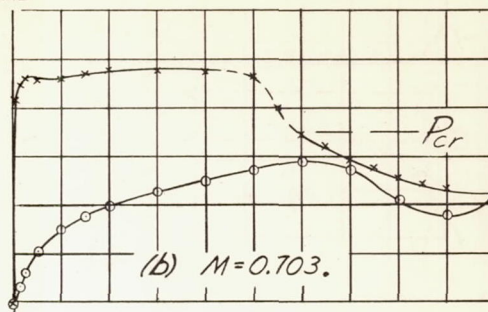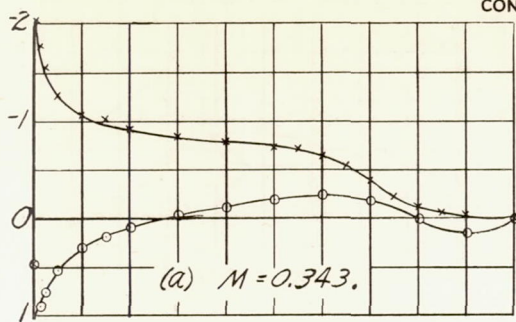
Fig. 19   NACA RM No. L6L16
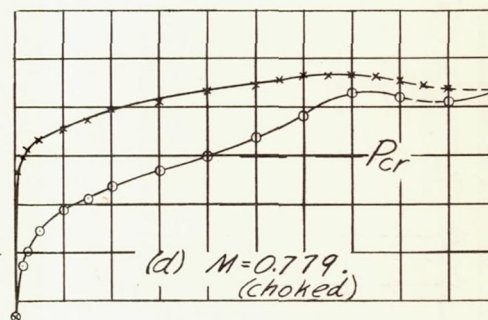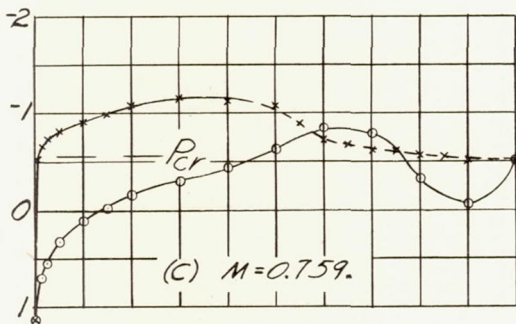
Figure 19.— Pressure distribution for the NACA 66,2-215 airfoil. α = 6°.
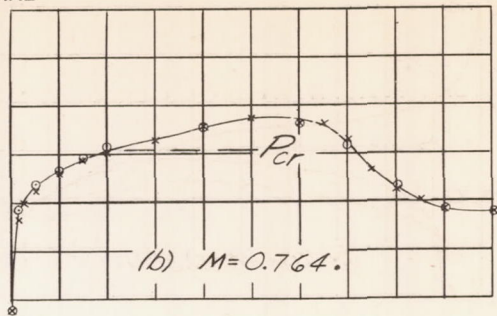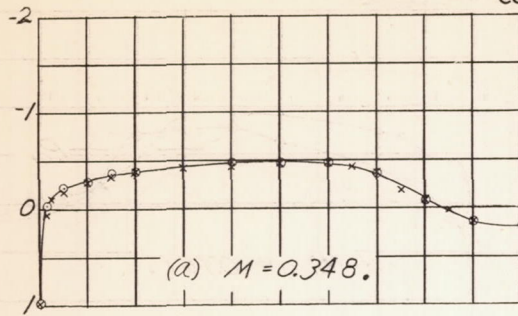
Pressure coefficient, P

(a) M = 0.348.

(b) M = 0.764.

P_{cr}

×   Upper surface
⊙   Lower surface

(c) M = 0.787.

P_{cr}

(d) M = 0.795.
(choked)

P_{cr}
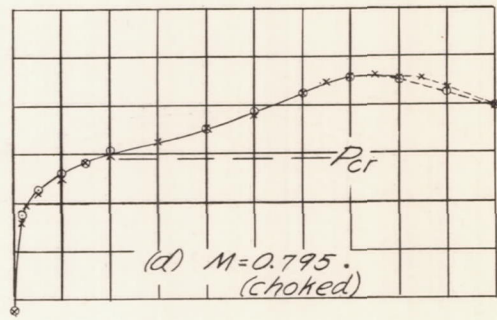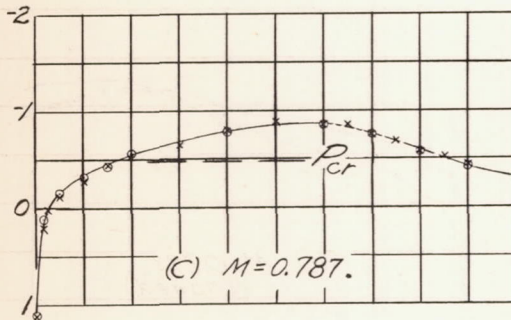
O   20   40   60   80   100   O   20   40   60   80   100
Percent chord

NATIONAL ADVISORY
COMMITTEE FOR AERONAUTICS

Figure 20.- Pressure distribution for the
NACA 66,2-015 airfoil.   α = 0°.
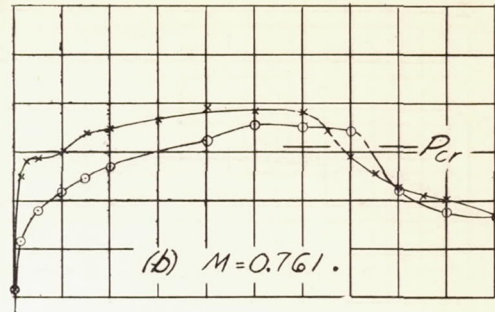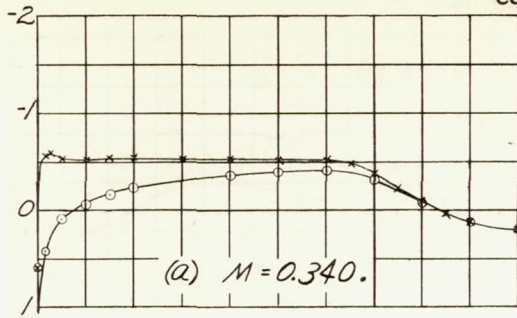
Fig. 21   NACA RM No. L6L16
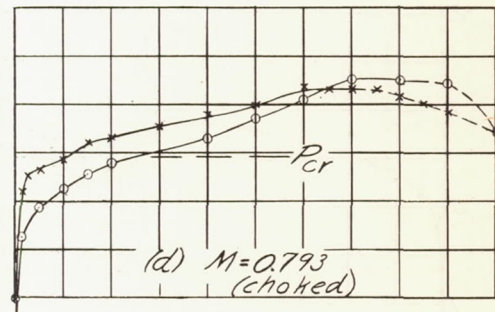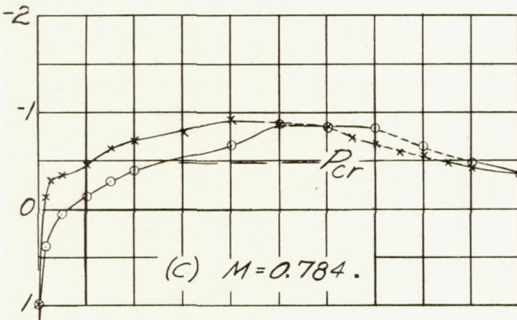
Figure 21.— Pressure distribution for the NACA 66,2-015 airfoil. α = 2°.

Figure 22.— Pressure distribution for the NACA 66,2-015 airfoil. α = 4°.
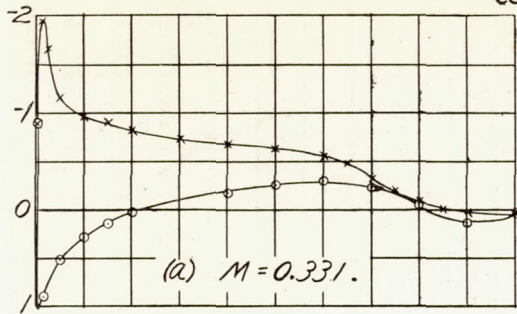
Fig. 23   NACA RM No. L6L16

CONFIDENTIAL

Pressure coefficient, P

(a) M = 0.331.

(b) M = 0.673.

× Upper surface
⊙ Lower surface

(c) M = 0.736.

(d) M = 0.777.
(choked)
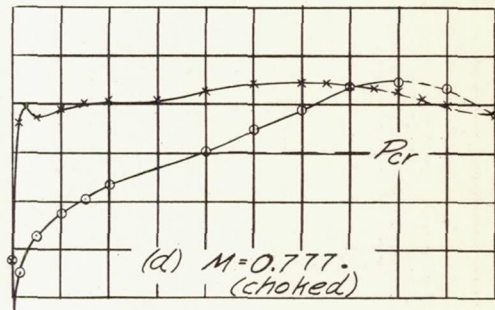
Percent chord

NATIONAL ADVISORY
COMMITTEE FOR AERONAUTICS

Figure 23.— Pressure distribution for the
NACA 66,2-015 airfoil. $\alpha = 6°$.
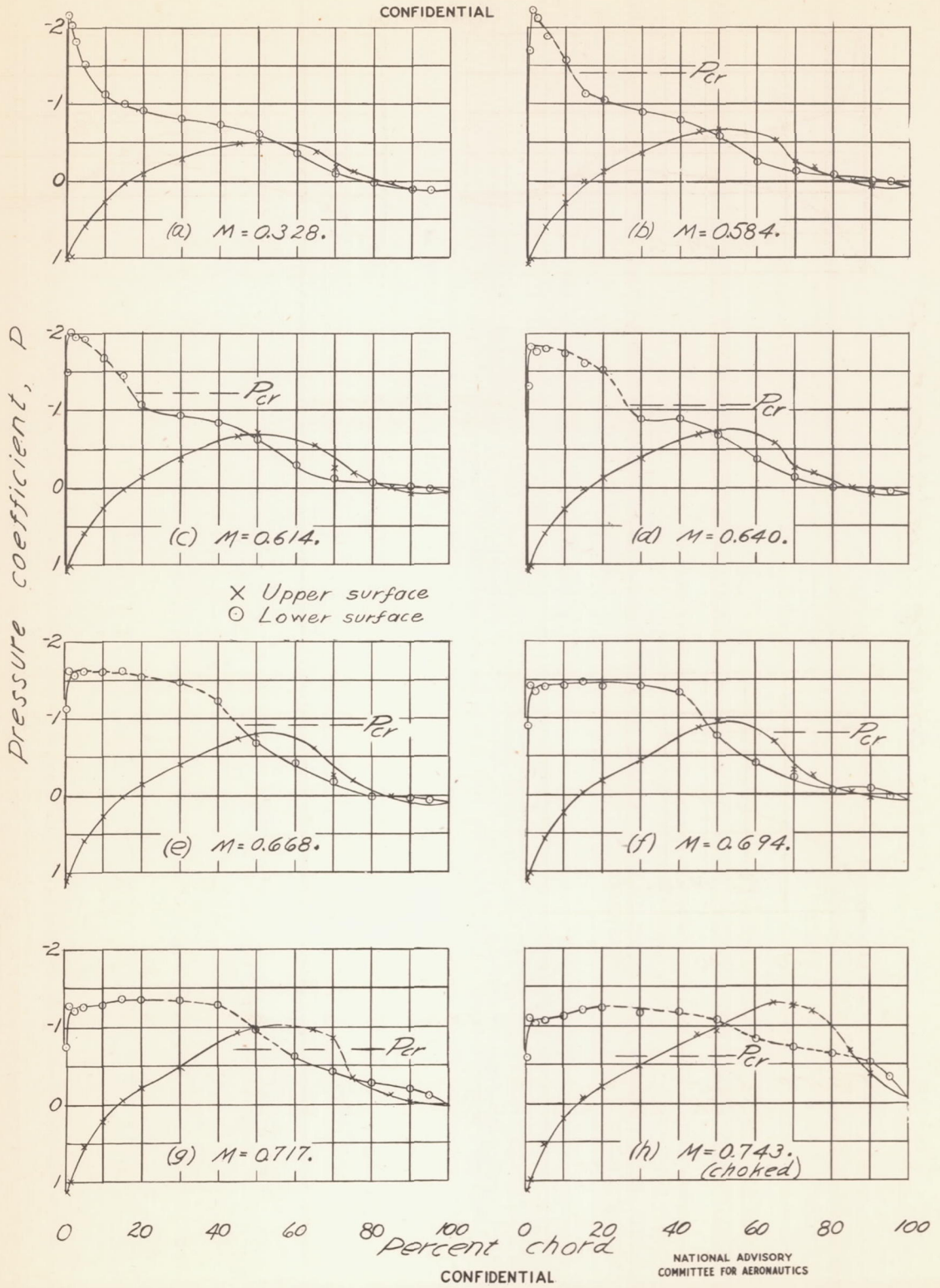
Figure 24.- Pressure distribution for the NACA 65(216)-418 airfoil. $\alpha = -6°$.
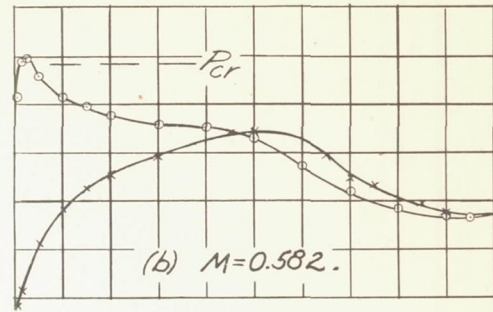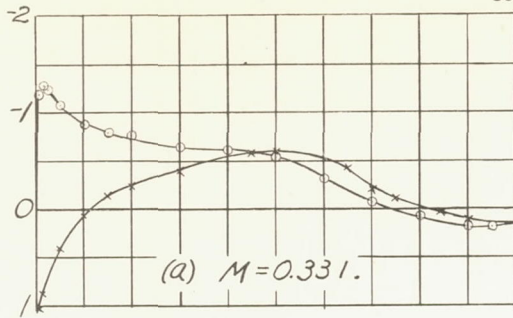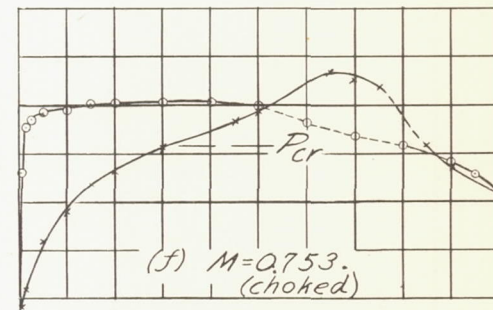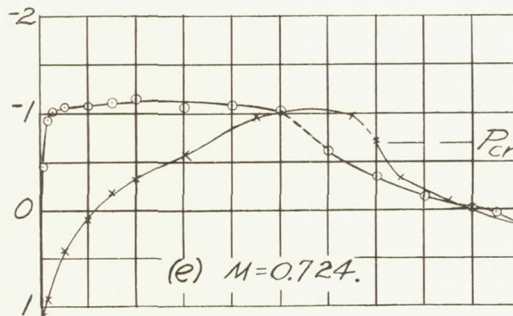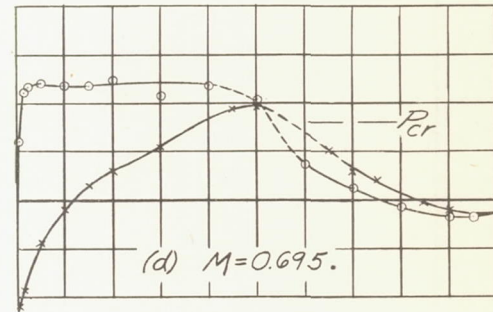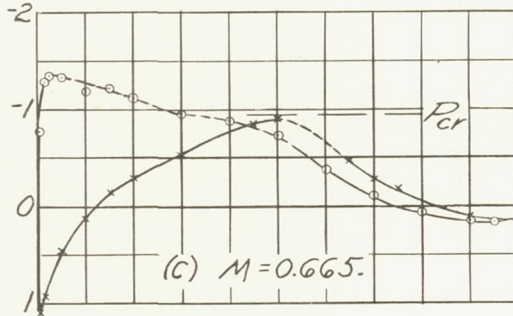
Fig. 25   NACA RM No. L6L16

Figure 25.- Pressure distribution for the NACA 65(216)-418 airfoil. $\alpha = -4°$.

CONFIDENTIAL
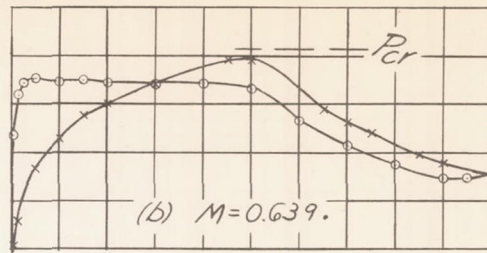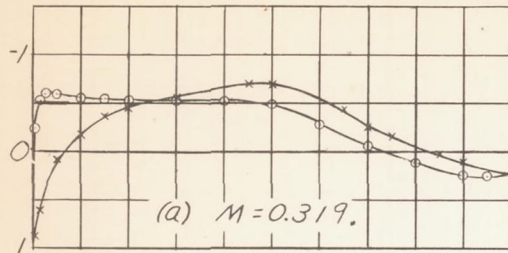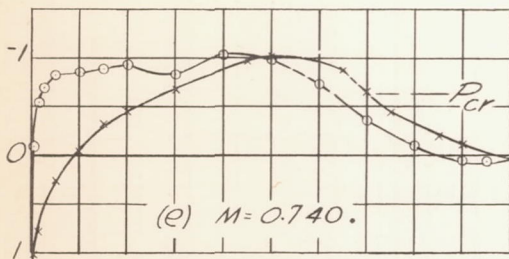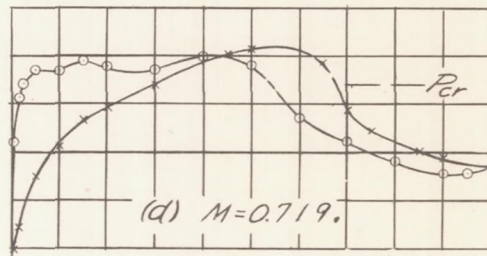
(a) M = 0.319.

(b) M = 0.639.

P_{cr}

× Upper surface
⊙ Lower surface

(c) M = 0.694.

P_{cr}

(d) M = 0.719.

P_{cr}

Pressure coefficient, P

(e) M = 0.740.

P_{cr}

(f) M = 0.761.
(choked)

P_{cr}

0   20   40   60   80   100   0   20   40   60   80   100

Percent chord

CONFIDENTIAL

NATIONAL ADVISORY
COMMITTEE FOR AERONAUTICS

Figure 26.- Pressure distribution for the
NACA 65(216)-418 airfoil. α = -2°
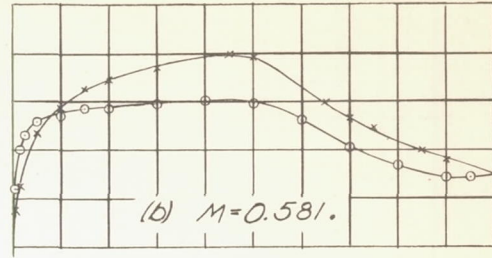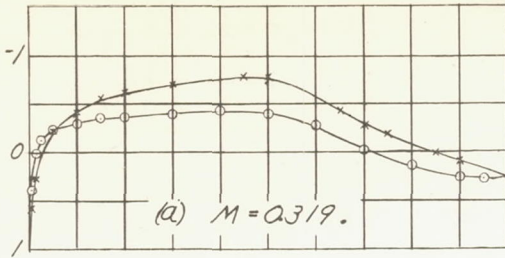
Fig. 27   NACA RM No. L6L16

Figure 27.— Pressure distribution for the NACA 65(216)-418 airfoil. α = 0°.
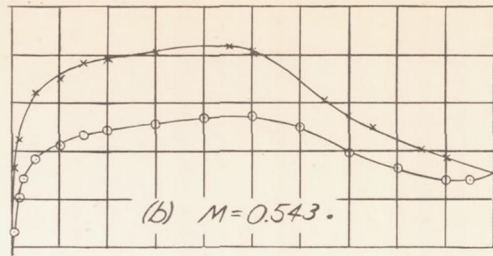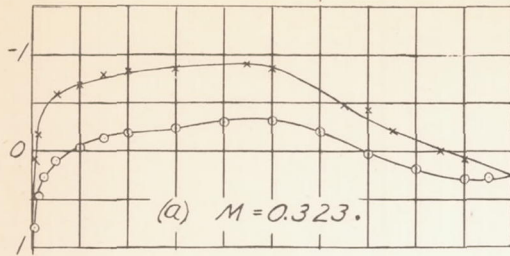
CONFIDENTIAL

Figure 28.- Pressure distribution for the NACA 65(216)-418 airfoil. $\alpha = 2°$.
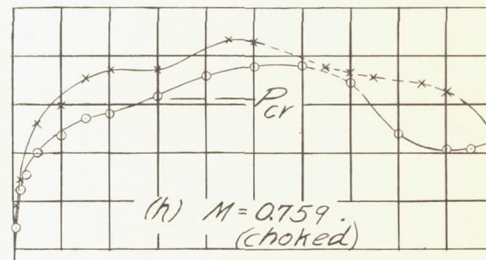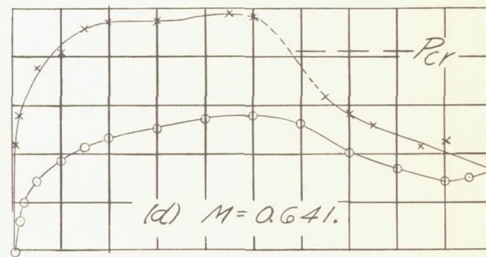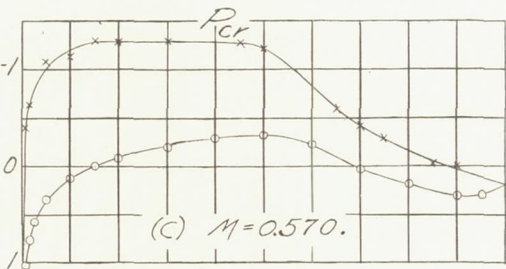
Fig. 29   NACA RM No. L6L16

CONFIDENTIAL

x upper surface
o Lower surface

Pressure coefficient, P

(a) M = 0.327.

(b) M = 0.469.

(c) M = 0.570.

(d) M = 0.641.

(e) M = 0.689.

(f) M = 0.715.

(g) M = 0.741

(h) M = 0.759.
     (choked)

0   20   40   60   80   100   0   20   40   60   80   100
Percent chord

CONFIDENTIAL

NATIONAL ADVISORY
COMMITTEE FOR AERONAUTICS

Figure 29.— Pressure distribution for the
NACA 65(216)-418 airfoil.   α = 4°

CONFIDENTIAL

(a) M = 0.446.

(b) M = 0.584.

x   Upper surface
o   Lower surface

Pcr

(c) M = 0.610.

Pcr

(d) M 0.665.

Pcr

(e) M = 0.719.

Pcr

(f) M = 0.748.
(choked)

Pressure coefficient, P

Percent chord

NATIONAL ADVISORY
COMMITTEE FOR AERONAUTICS

CONFIDENTIAL

Figure 30.— Pressure distribution for the
NACA 65(216)-418 airfoil. α = 6°.
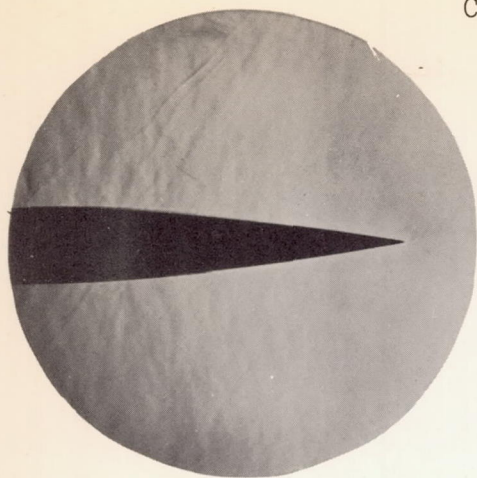
(a) M = 0.577.
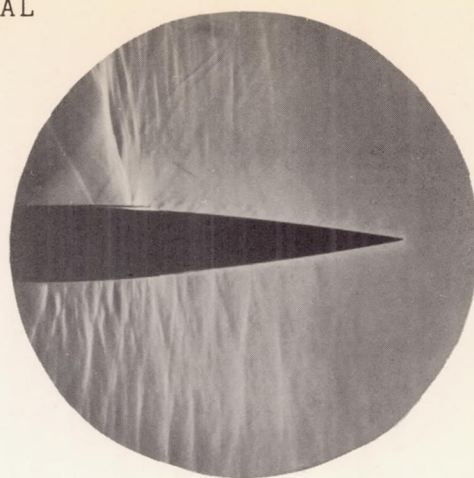
(b) M = 0.742.
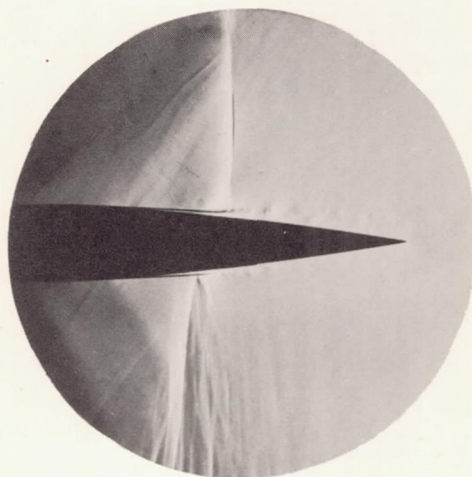
(c) M = 0.769.
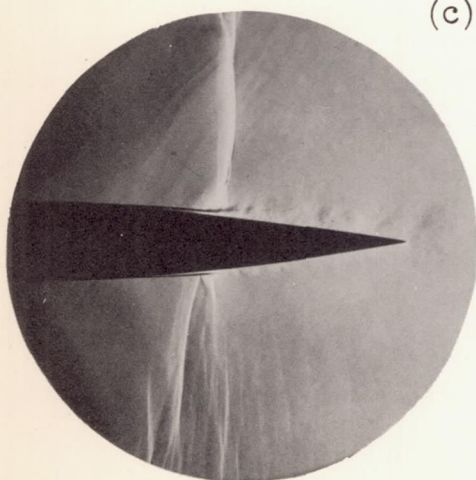
(d) M = 0.774.
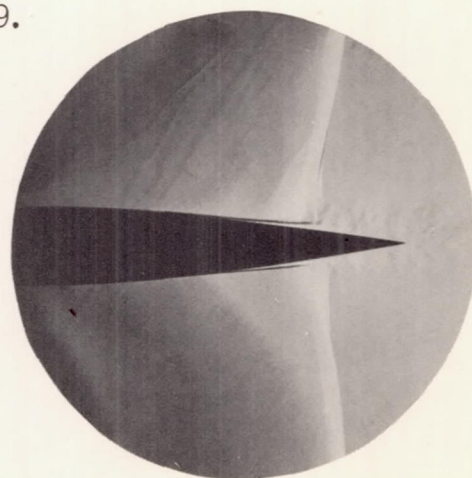
(e) M = 0.780 (choked).

Figure 31.- Schlieren photographs of the NACA 23015 airfoil. α = 0°.
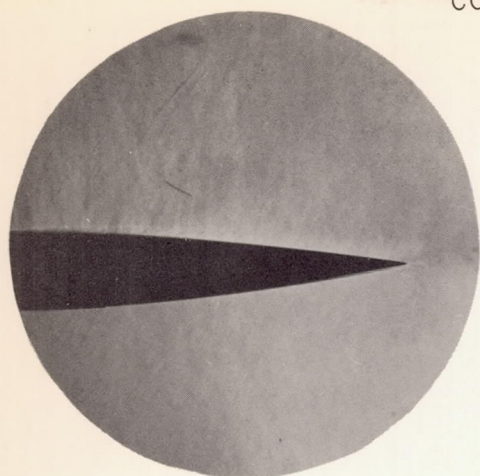
(a)   M = 0.524.
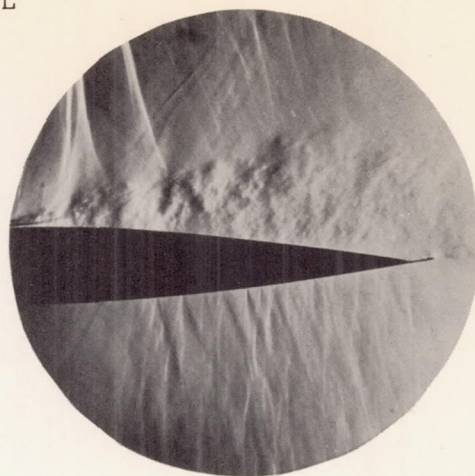
(b)   M = 0.731.
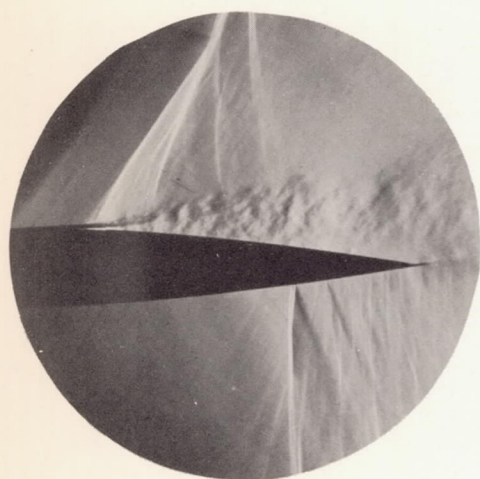
(c)   M = 0.756.
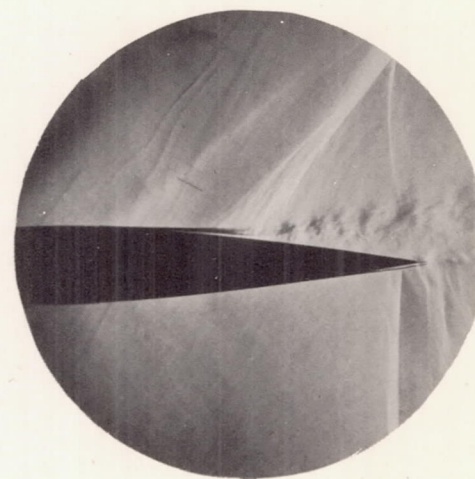
(d)   M = 0.762 (choked).

Figure 32.- Schlieren photographs of the NACA 23015 airfoil. $\alpha = 6^{\circ}$.
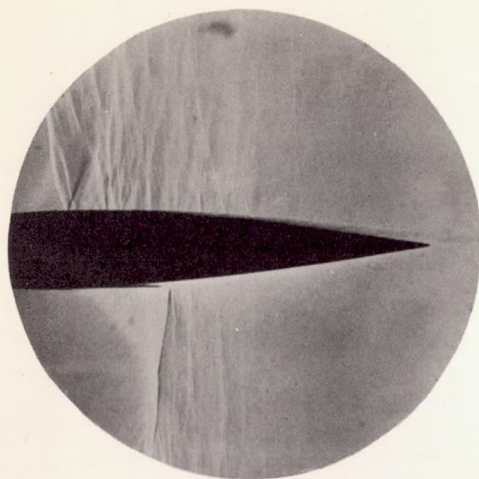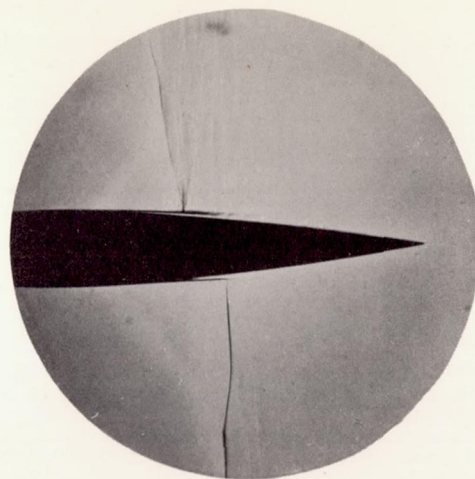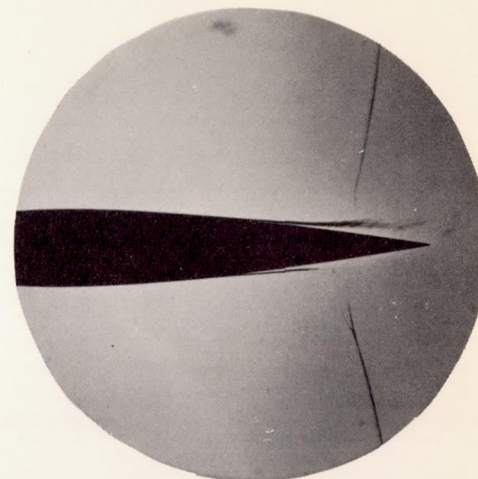
(a) M = 0.752.   (b) M = 0.777.   (c) M = 0.781.

Figure 33.- Schlieren photographs of the NACA 23015 airfoil. $\alpha = -2^{\circ}$.

NATIONAL ADVISORY COMMITTEE FOR AERONAUTICS
LANGLEY MEMORIAL AERONAUTICAL LABORATORY — LANGLEY FIELD, VA.

Fig. 33
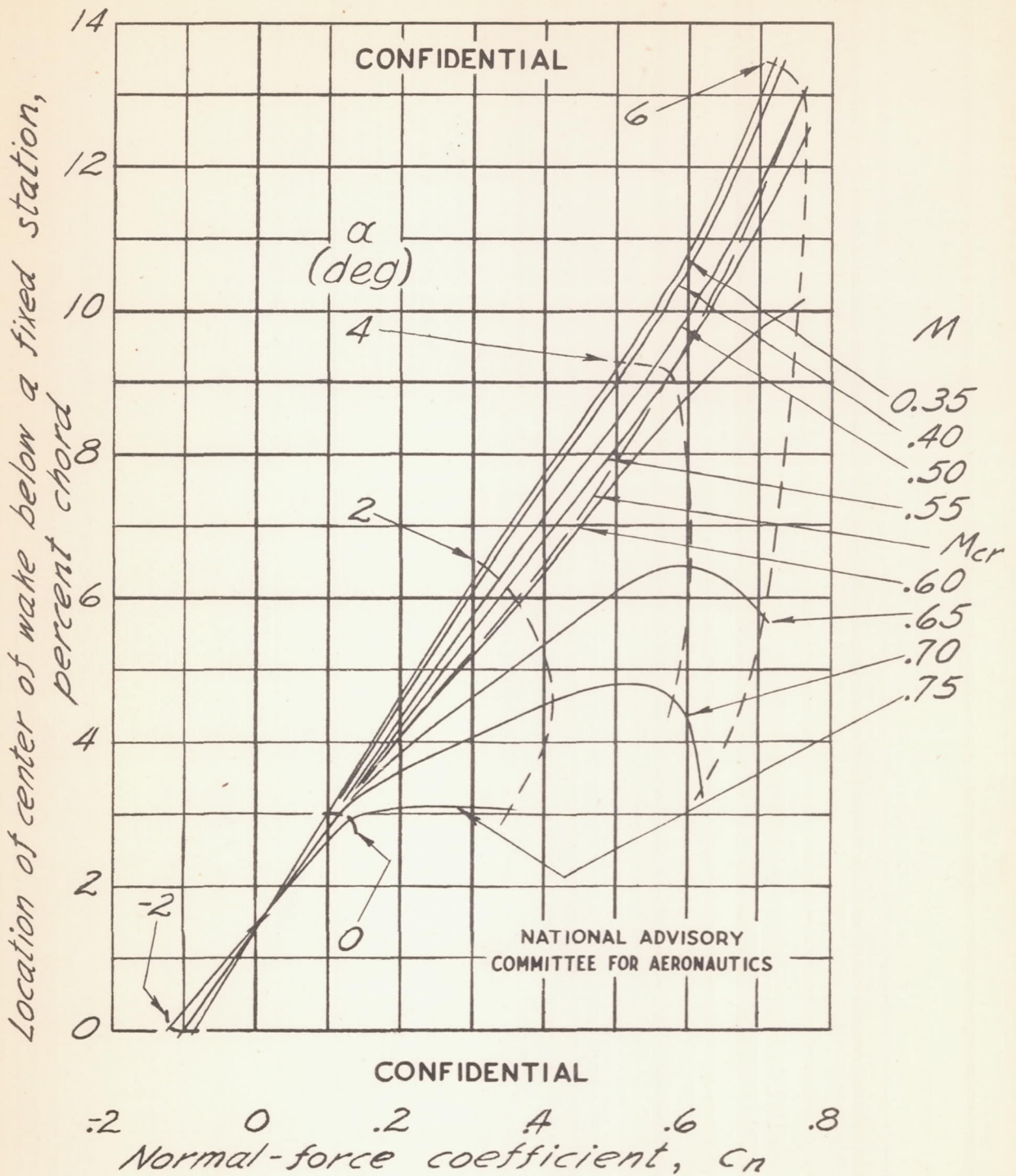
Figure 34.— Variation with normal-force coefficient of the center of the wake of an NACA 23015 airfoil. Rake location is 0.5 chord from the trailing edge.

Fig. 35   NACA RM No. L6L16
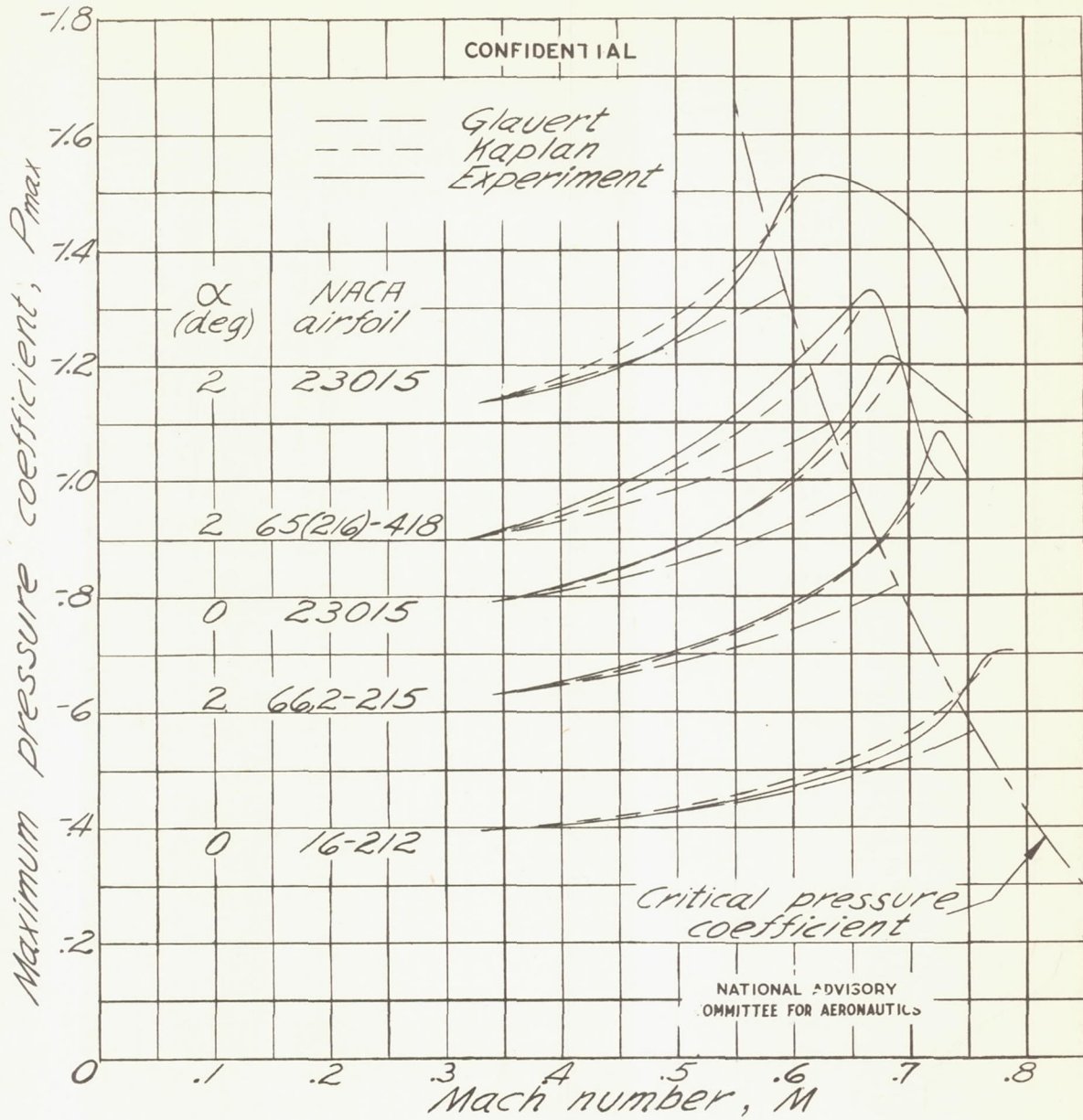
Figure 35.— A comparison with theory of the variation of maximum pressure coefficient with Mach number for several airfoils.

Fig. 36
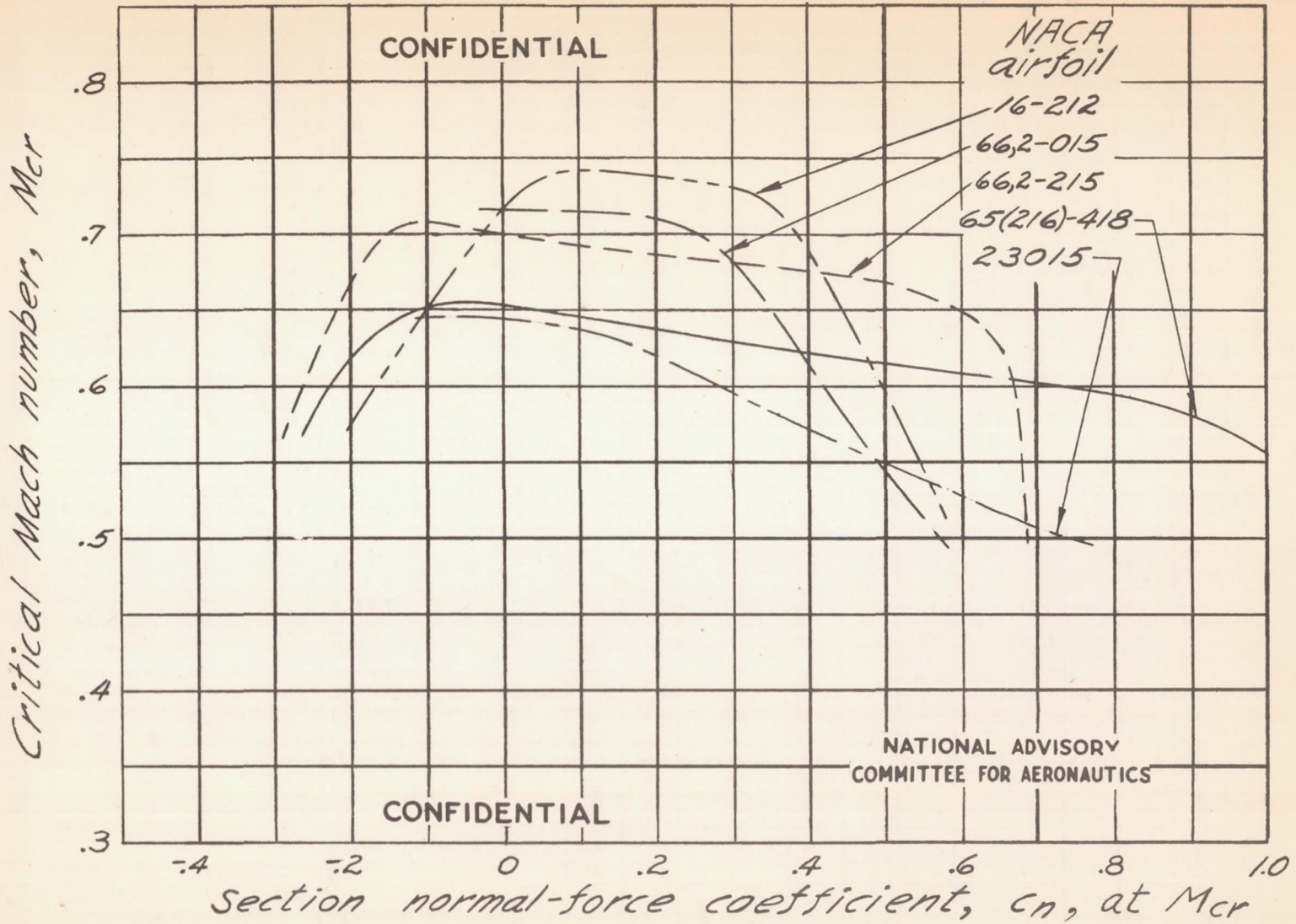
Figure 36.— Variation of critical Mach number with normal-force coefficient for each airfoil.

Fig. 37   NACA RM No. L6L16
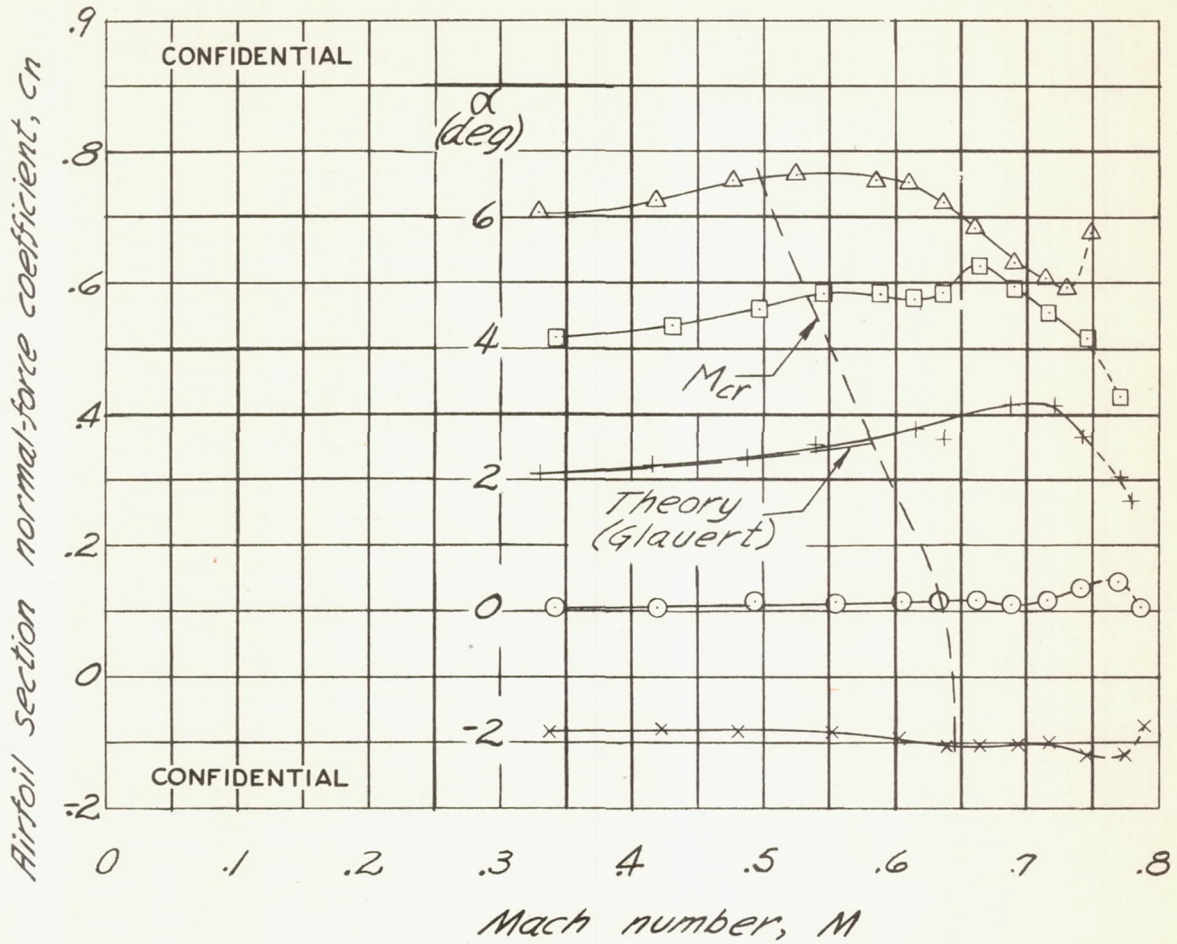
Figure 37.— Variation of section normal-force coefficient with Mach number for the NACA 23015 airfoil.
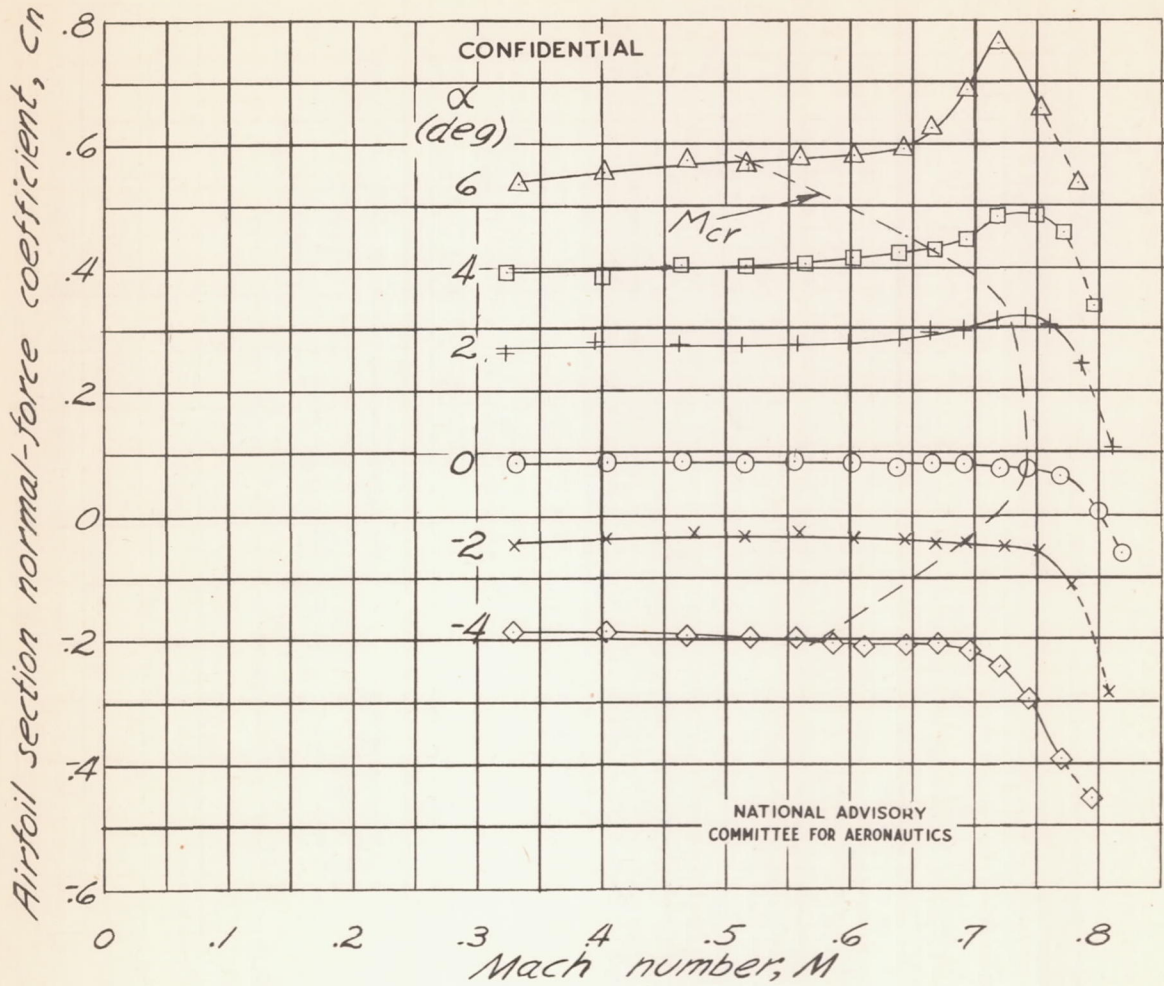
Figure 38.— Variation of section normal-force coefficient with Mach number for the NACA 16-212 airfoil.

Fig. 39   NACA RM No. L6L16
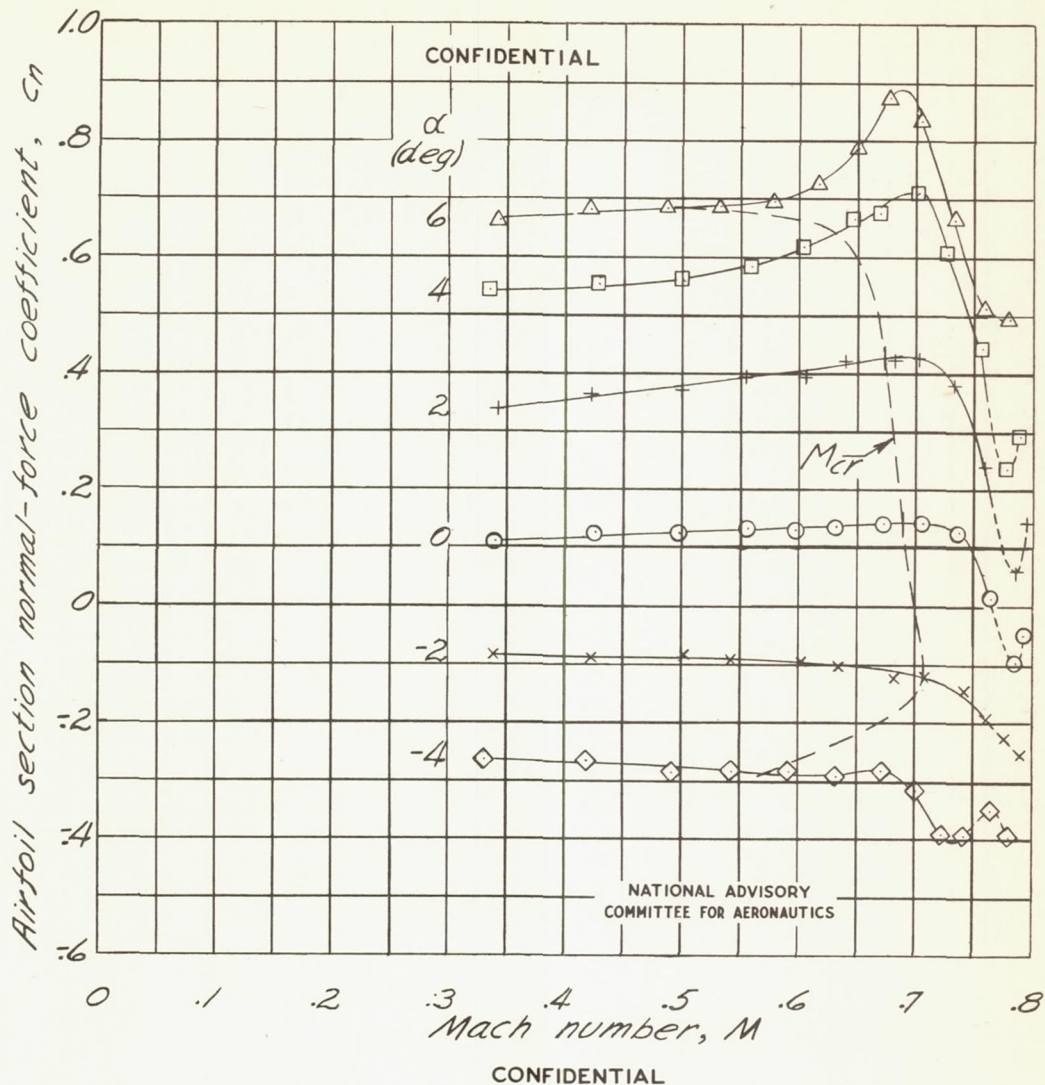
Figure 39.— Variation of section normal-force coefficient with Mach number for the NACA 66,2-215 airfoil.
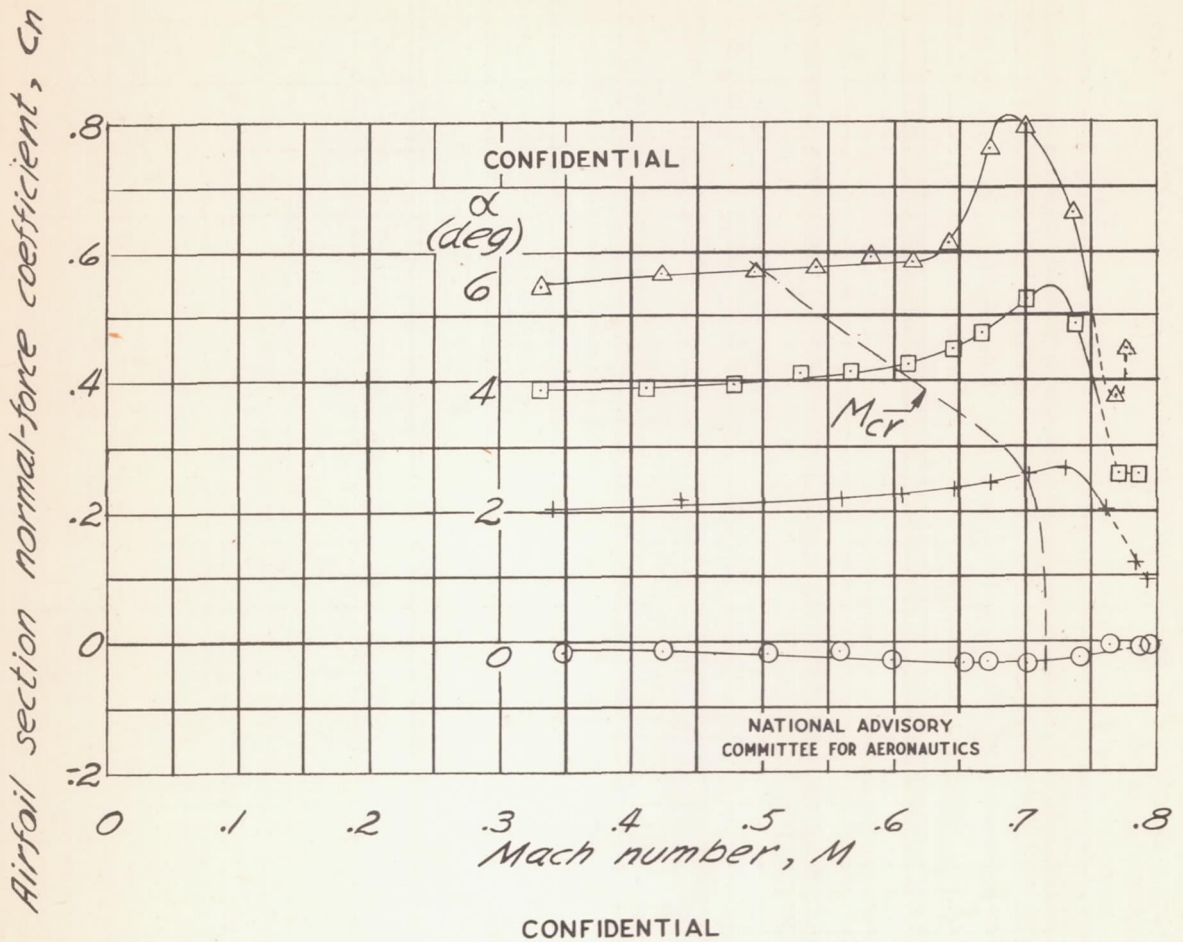
Figure 40. – Variation of section normal-force coefficient with Mach number for the NACA 66,2-015 airfoil.

Fig. 41   NACA RM No. L6L16
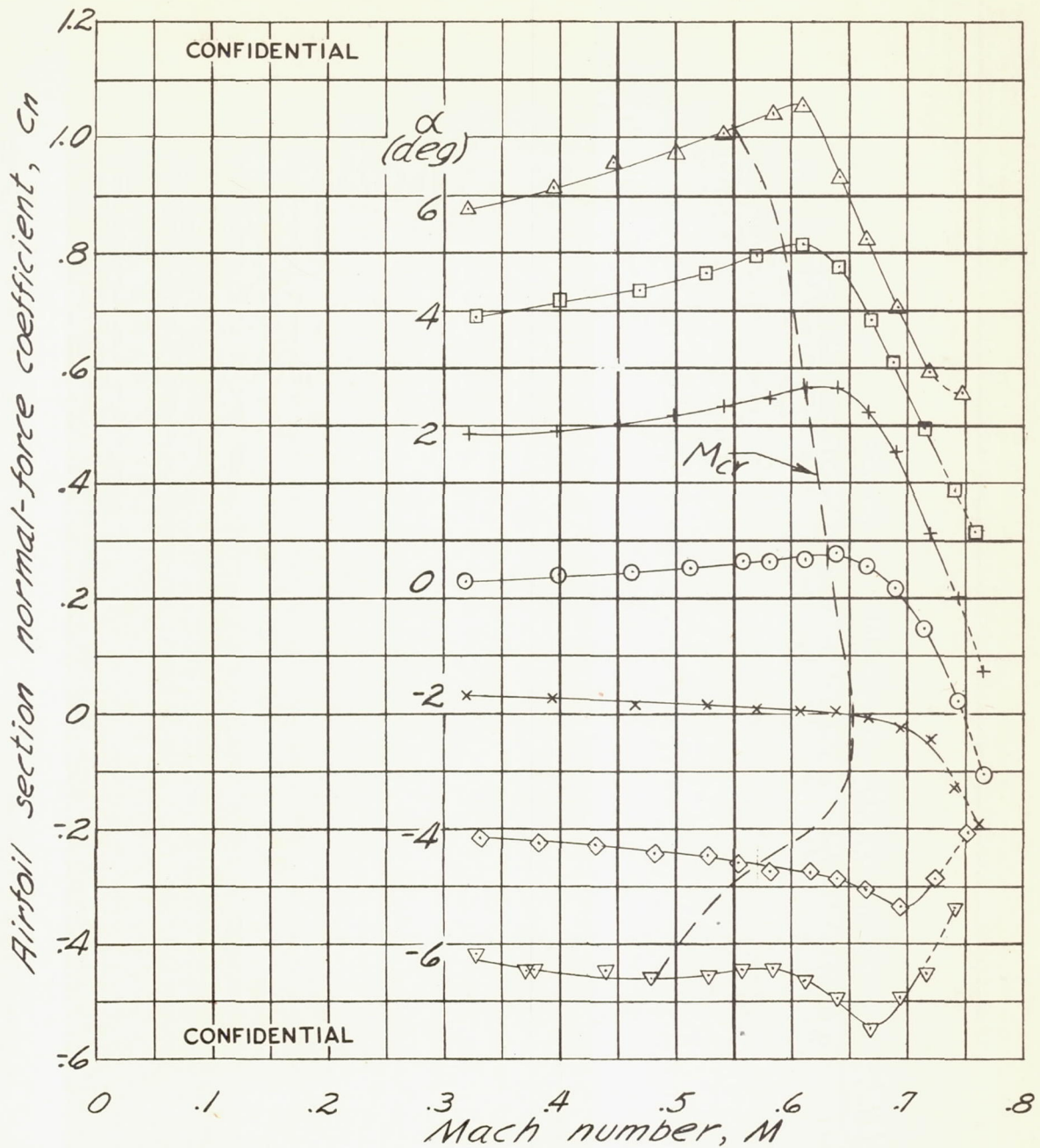
Figure 41.— Variation of section normal-force
coefficient with Mach number
for the NACA 65(216)-418 airfoil.
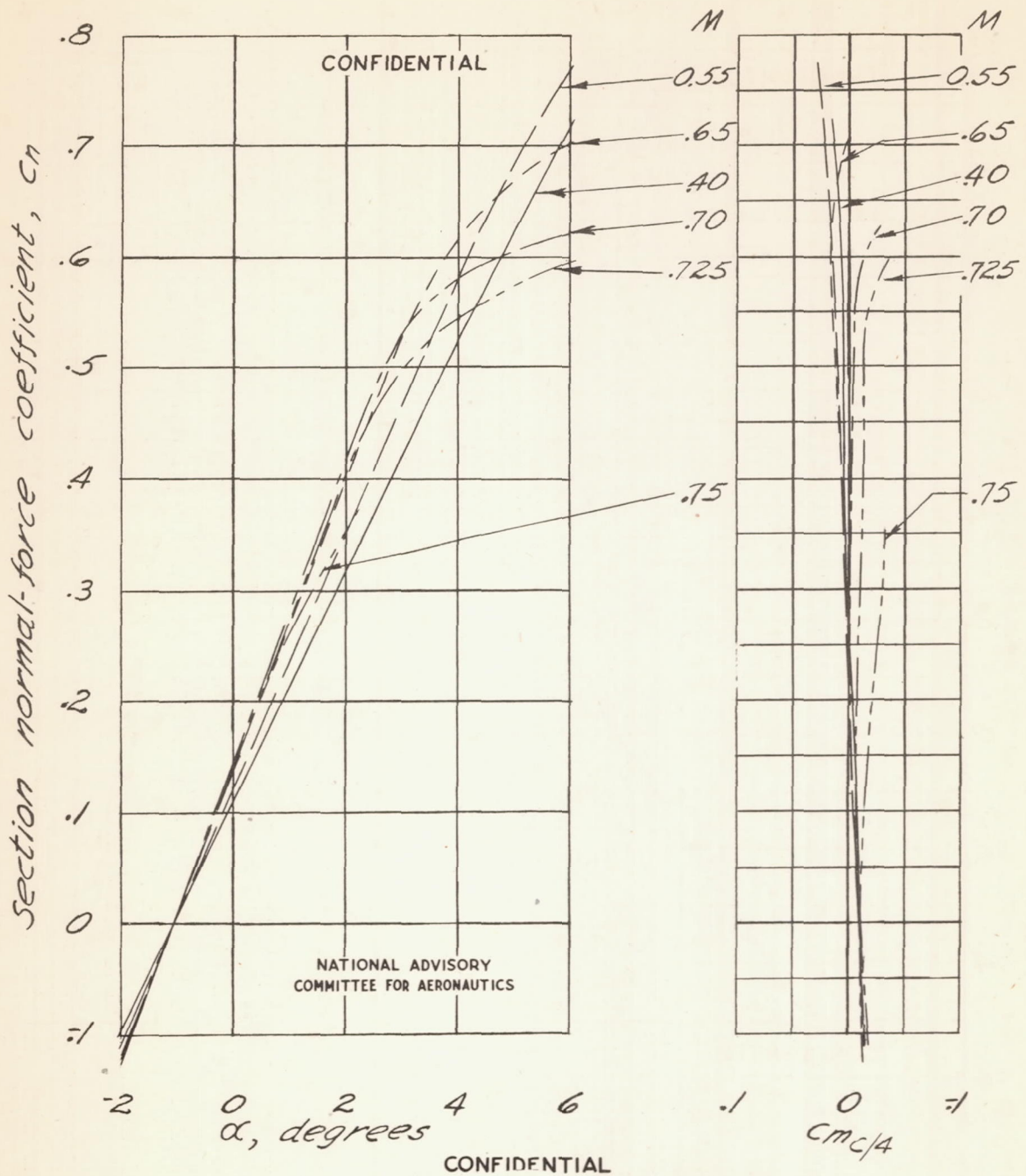
Figure 42.- Aerodynamic characteristics of the NACA 23015 airfoil.

Fig. 43   NACA RM No. L6L16
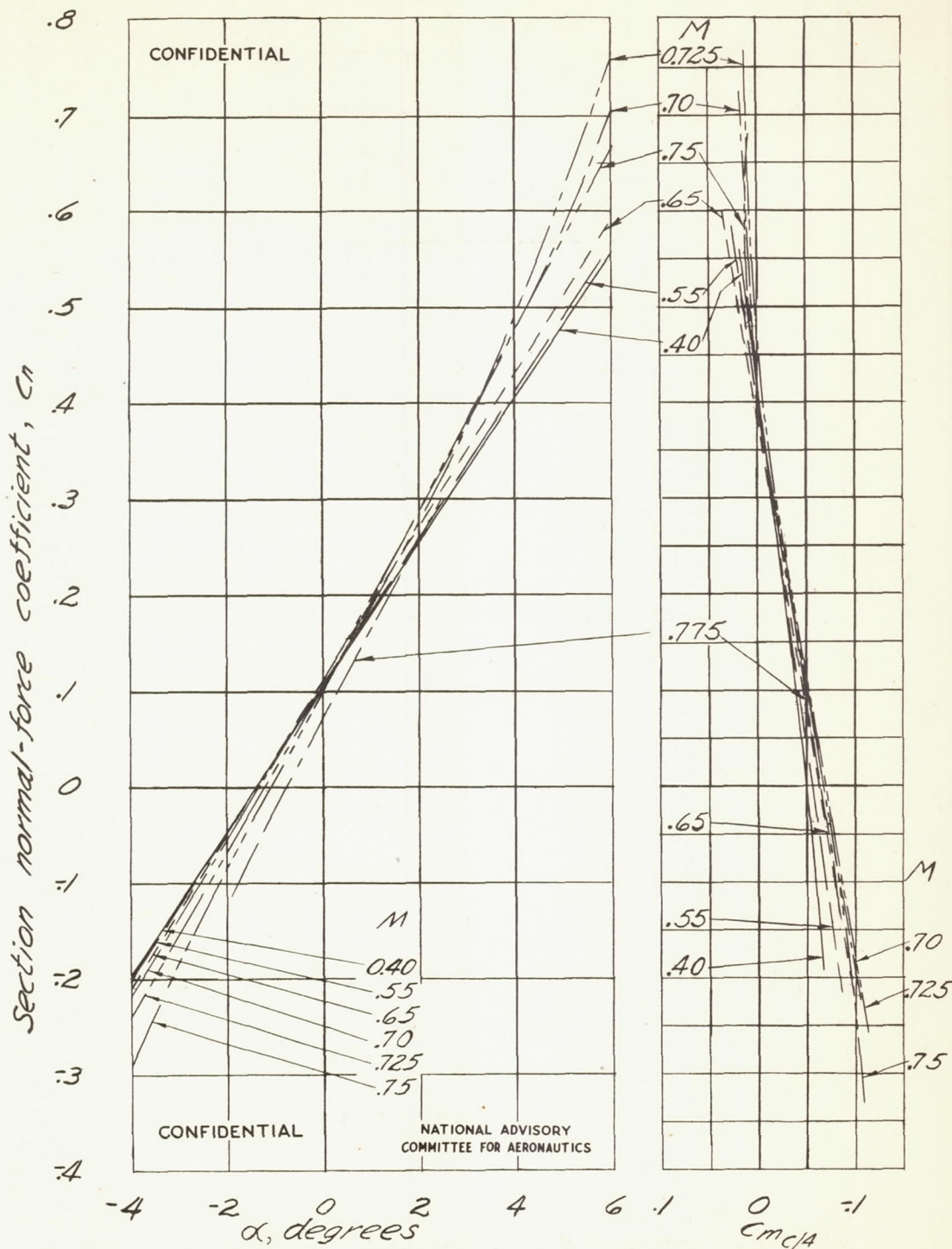
Figure 43.— Aerodynamic characteristics of
the NACA 16-212 airfoil.
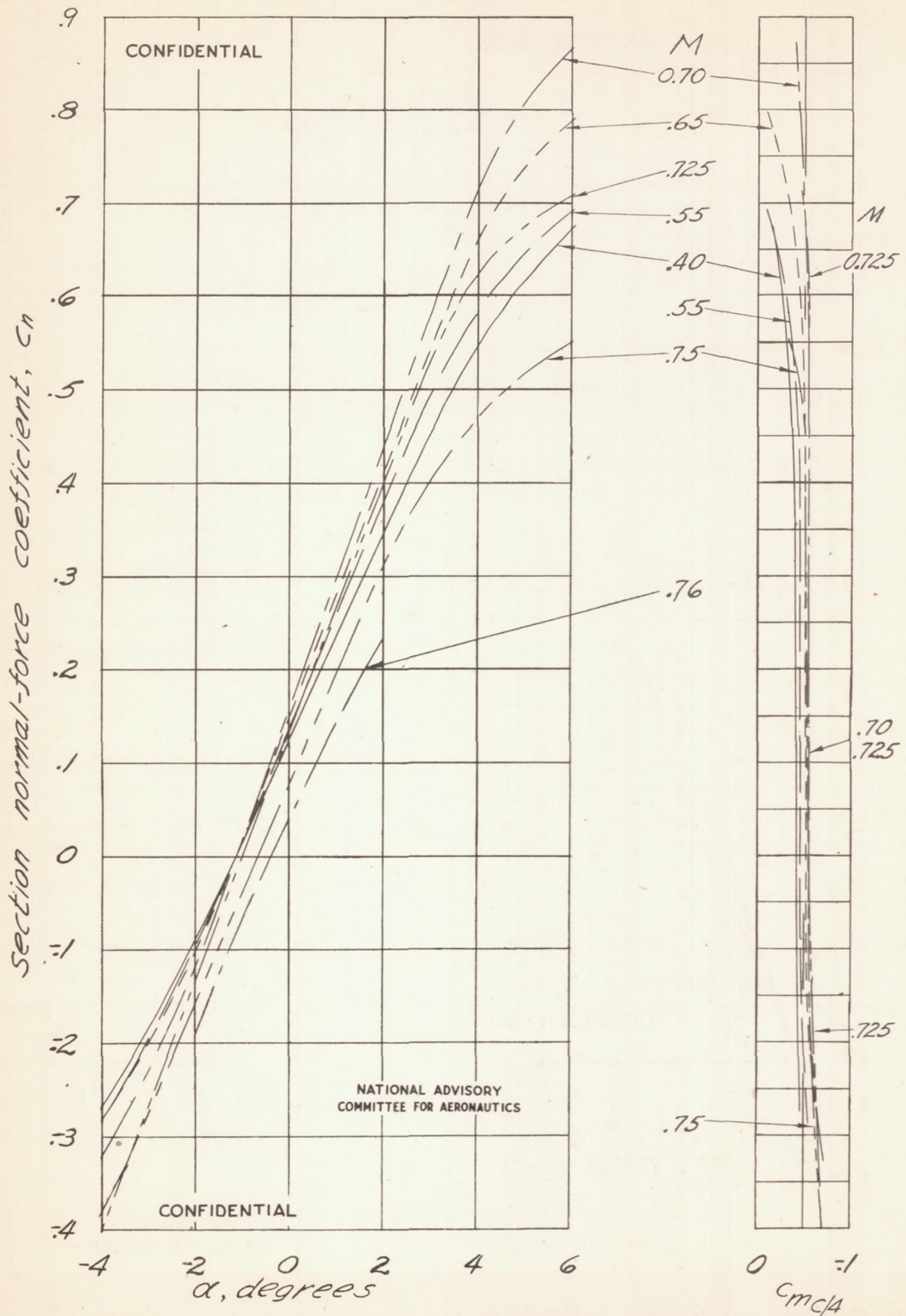
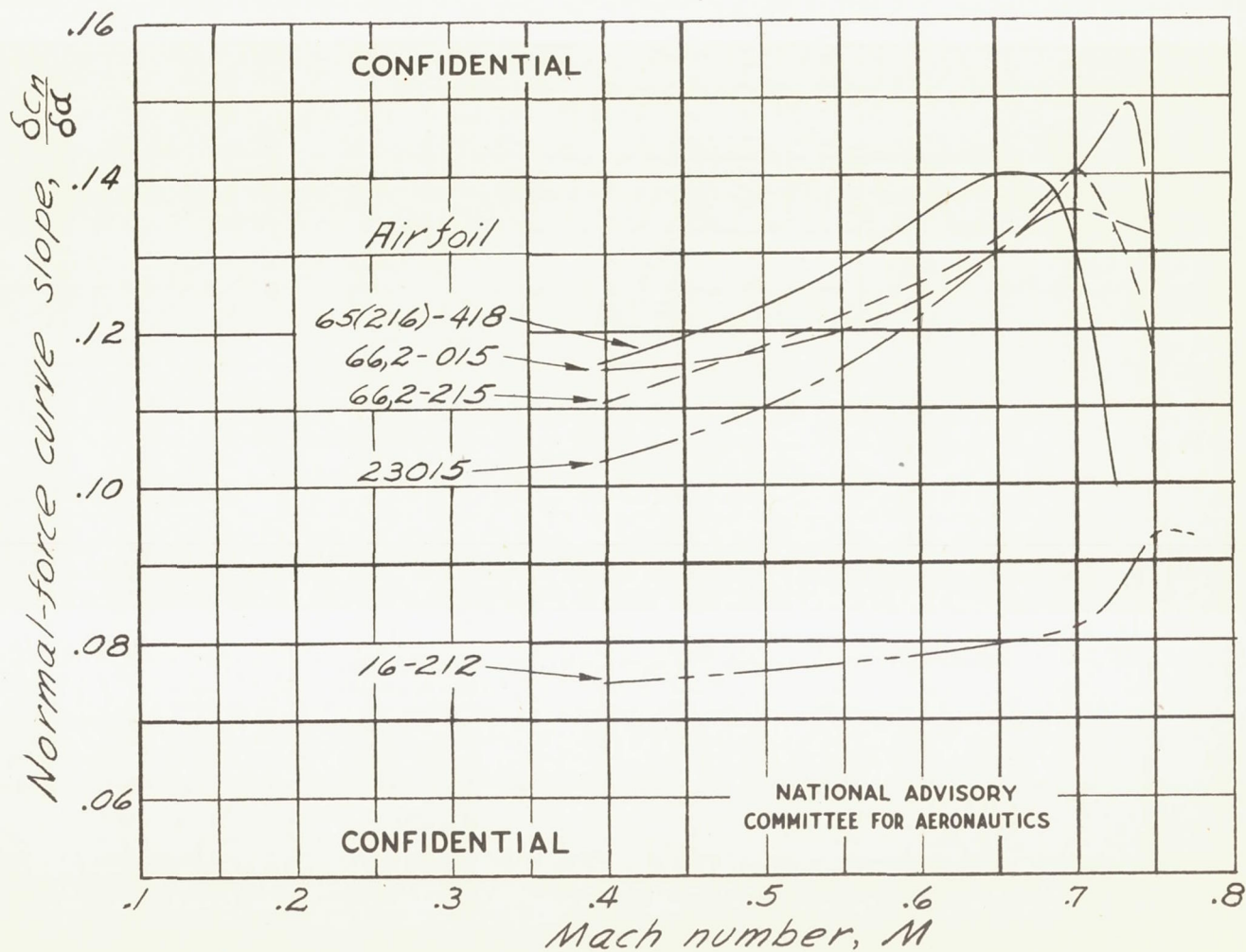Figure 44.— Aerodynamic characteristics
of the NACA 66,2-215 airfoil.

Fig. 45   NACA RM No. L6L16
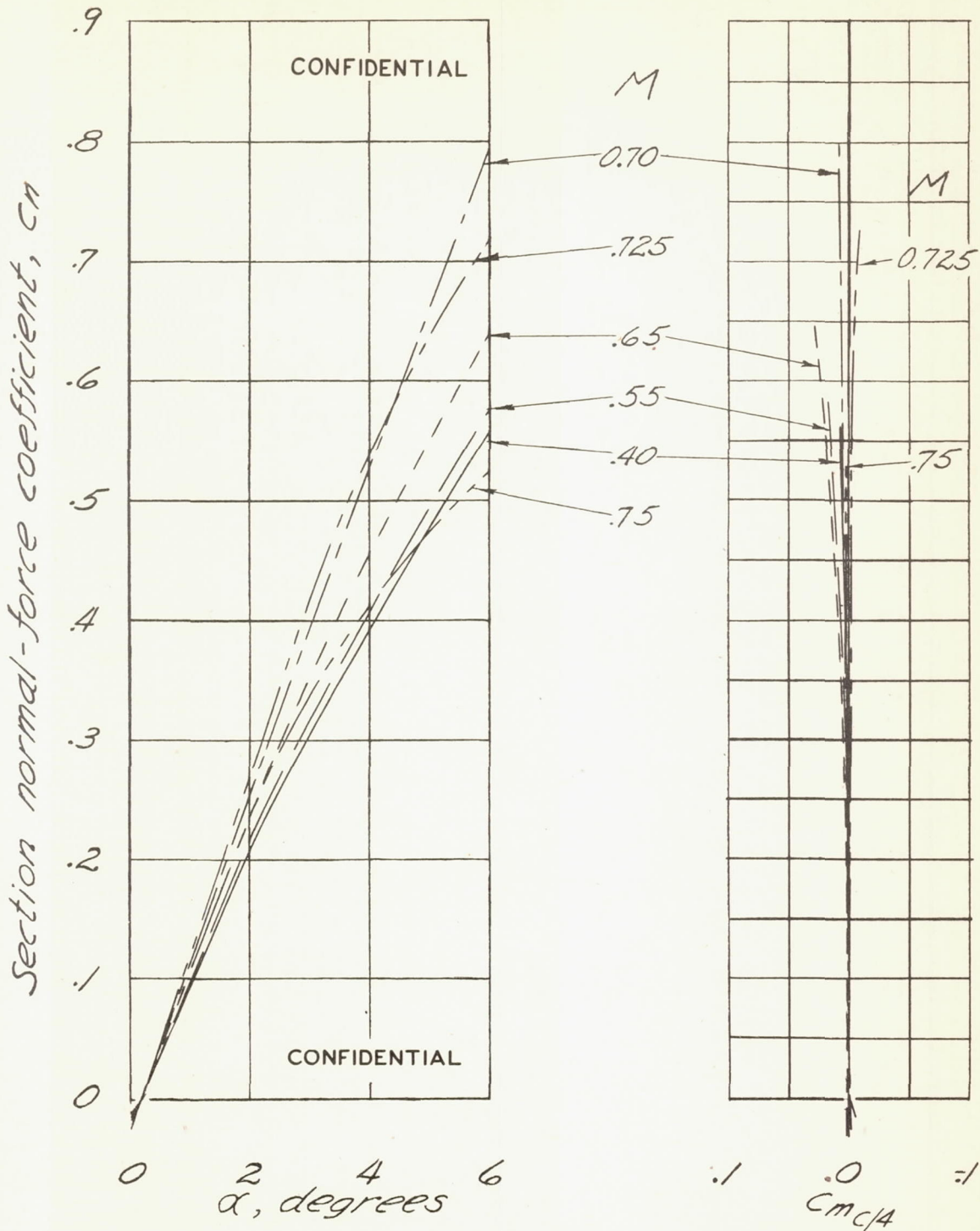
Figure 45.– Aerodynamic characteristics of the NACA 66,2-015 airfoil.
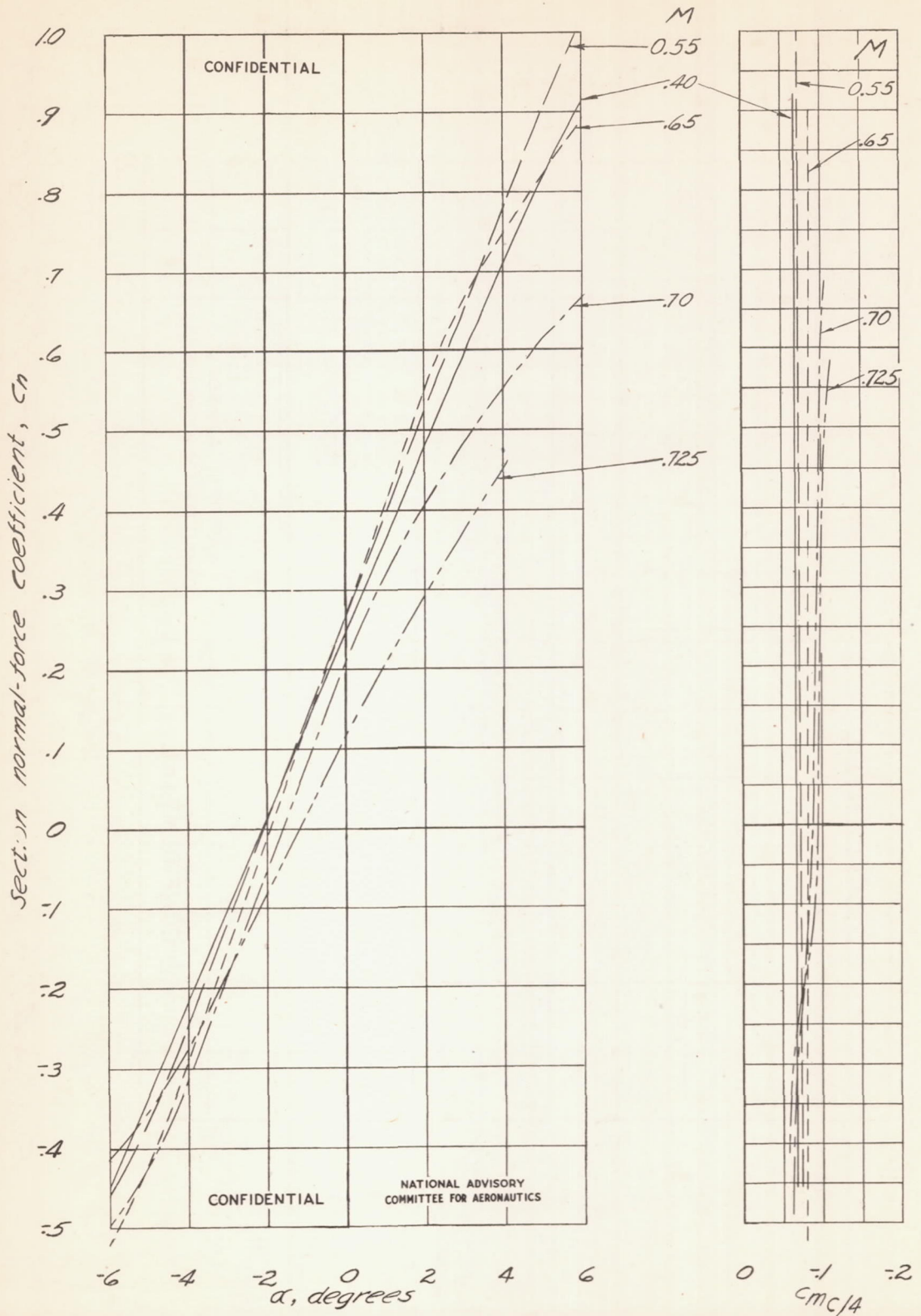
Figure 46.— Aerodynamic characteristics of the NACA 65(216)-418 airfoil.

Fig. 47

Figure 47.— Variation with Mach number of the slope of the curve of normal-force coefficient against angle of attack for each airfoil.
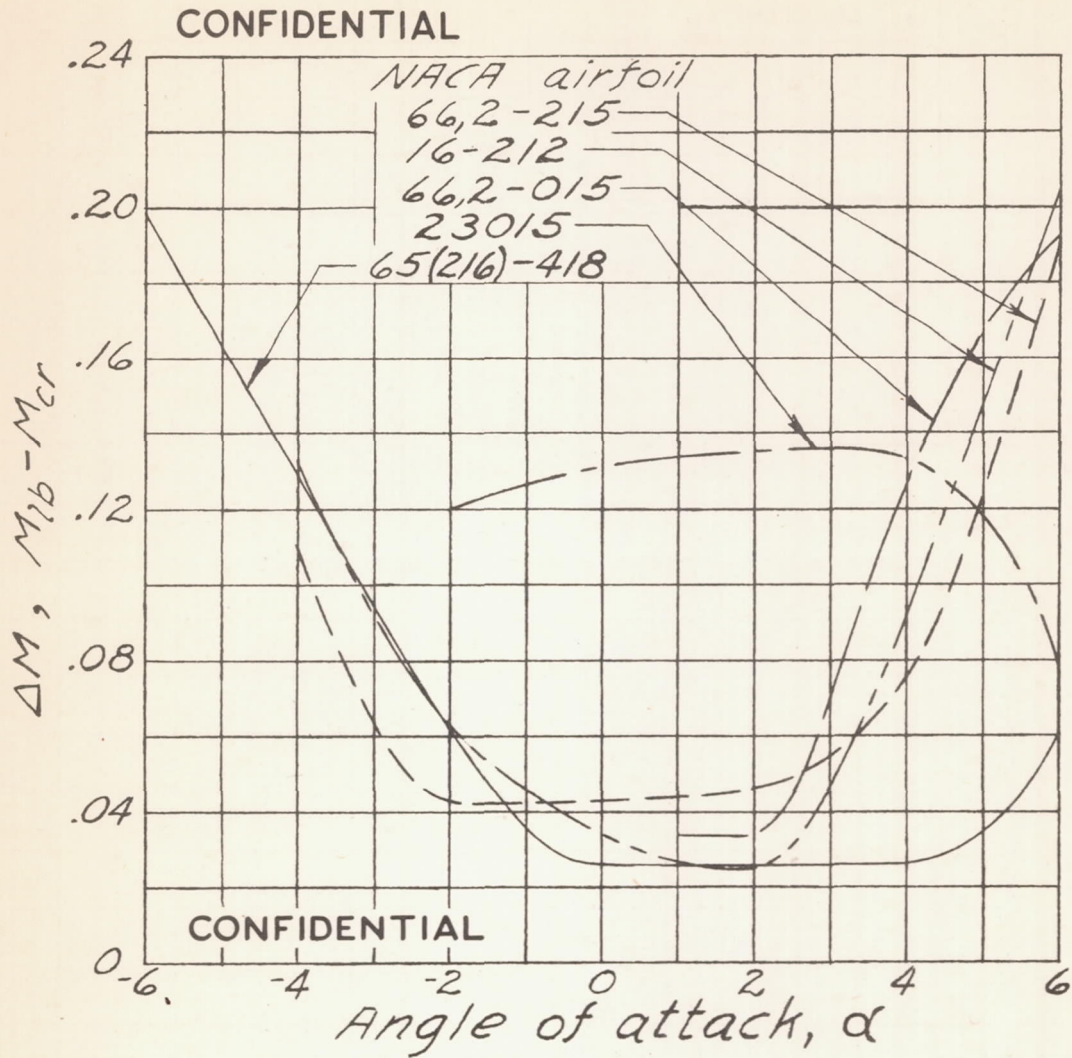
Figure 48.— Mach number increment, ΔM, by which the critical speed may be exceeded without incurring rapid changes in normal-force coefficient.
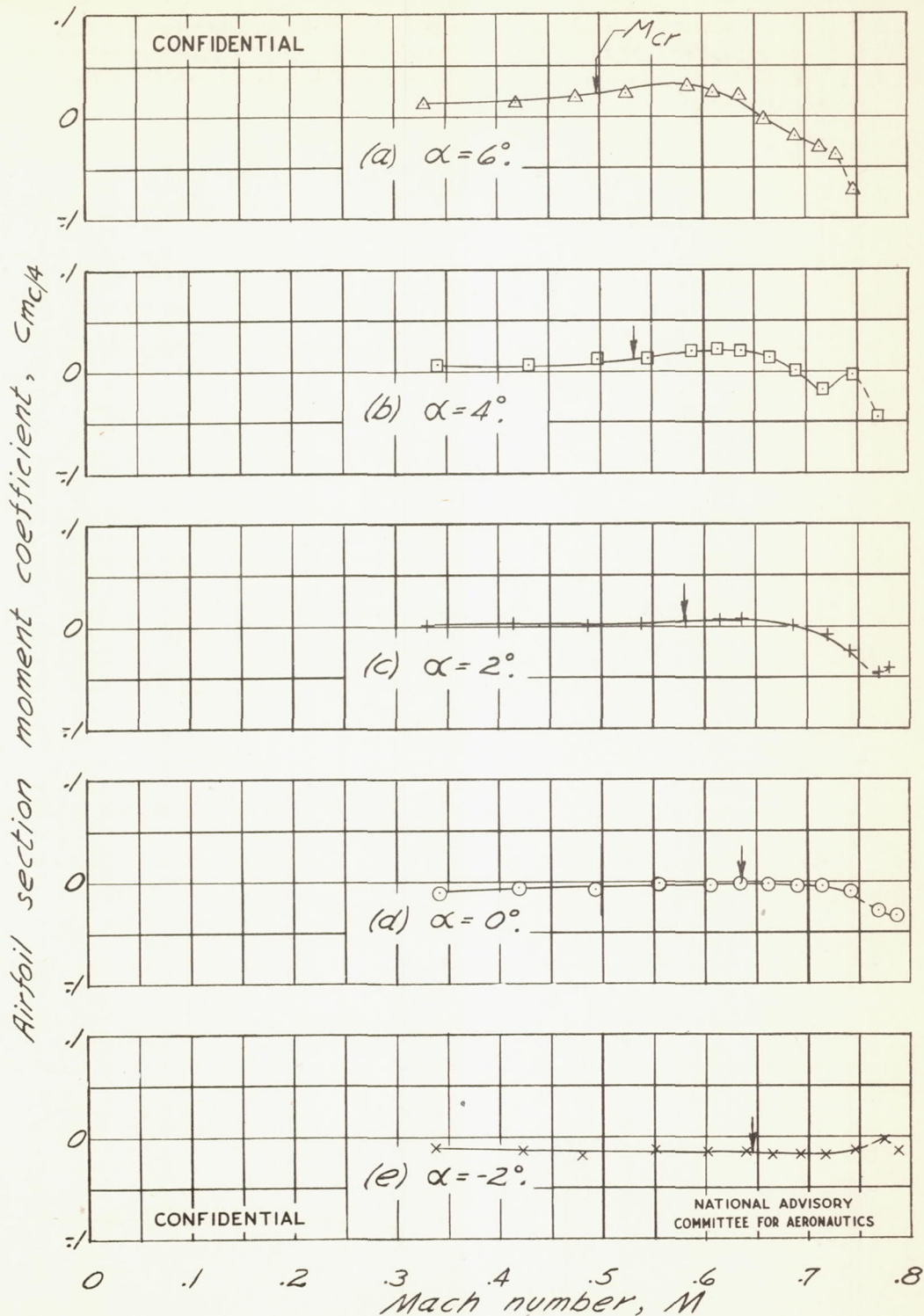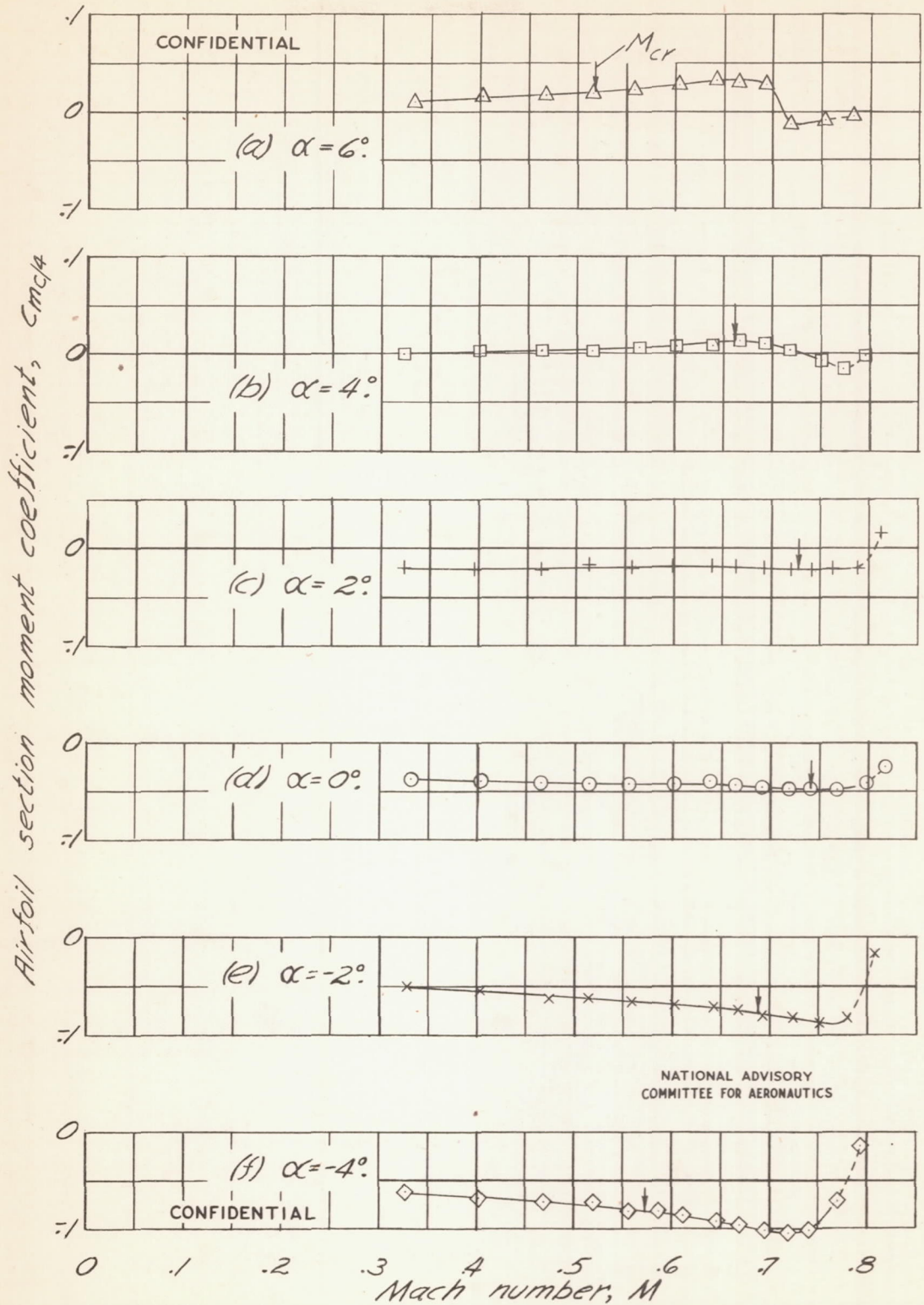
Fig. 49   NACA RM No. L6L16

Figure 49.— Variation of section moment coefficient with Mach number for the NACA 23015 airfoil.

Figure 50.— Variation of section moment
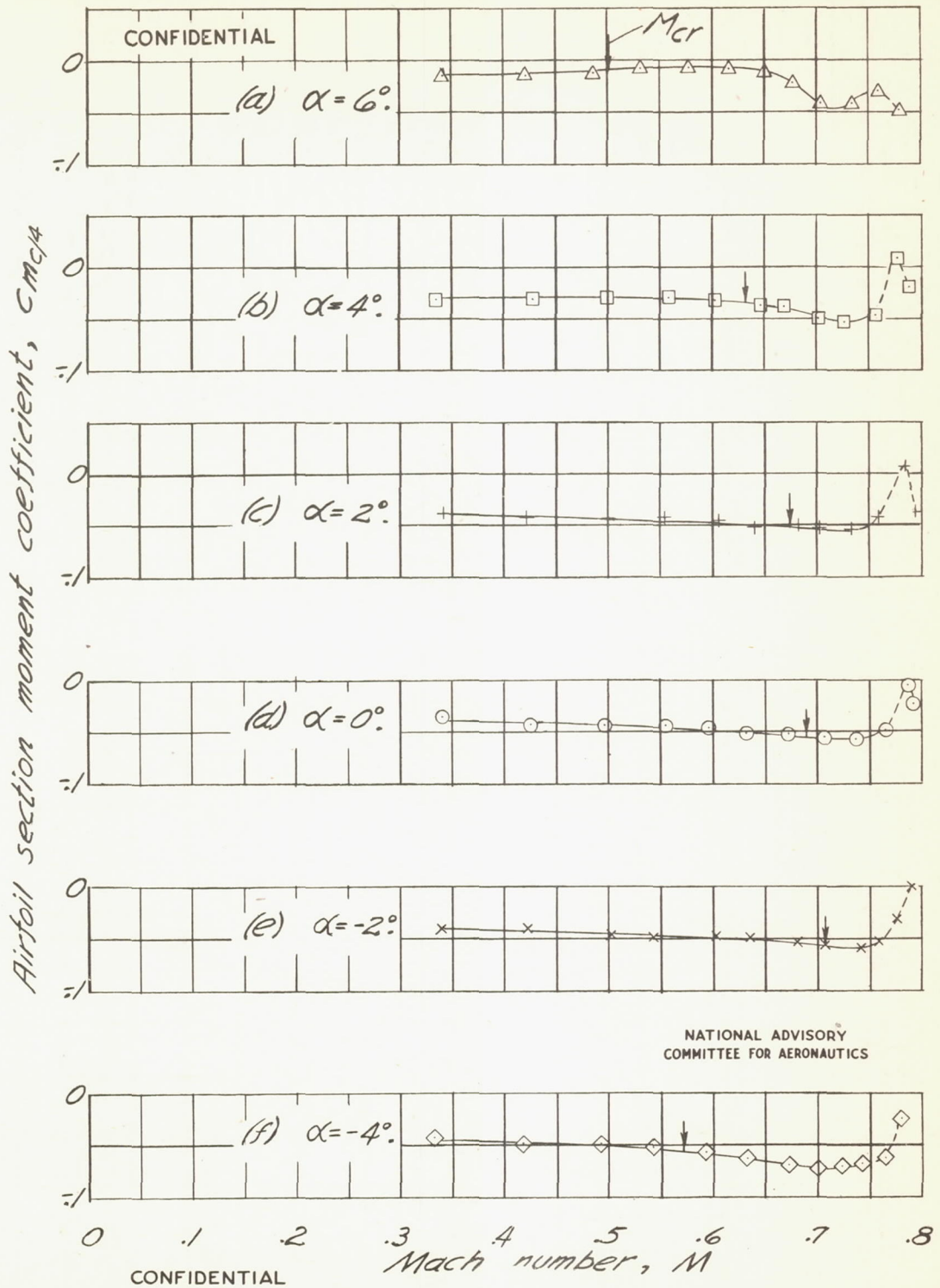coefficient with Mach number
for the NACA 16-212 airfoil.

Fig. 51   NACA RM No. L6L16
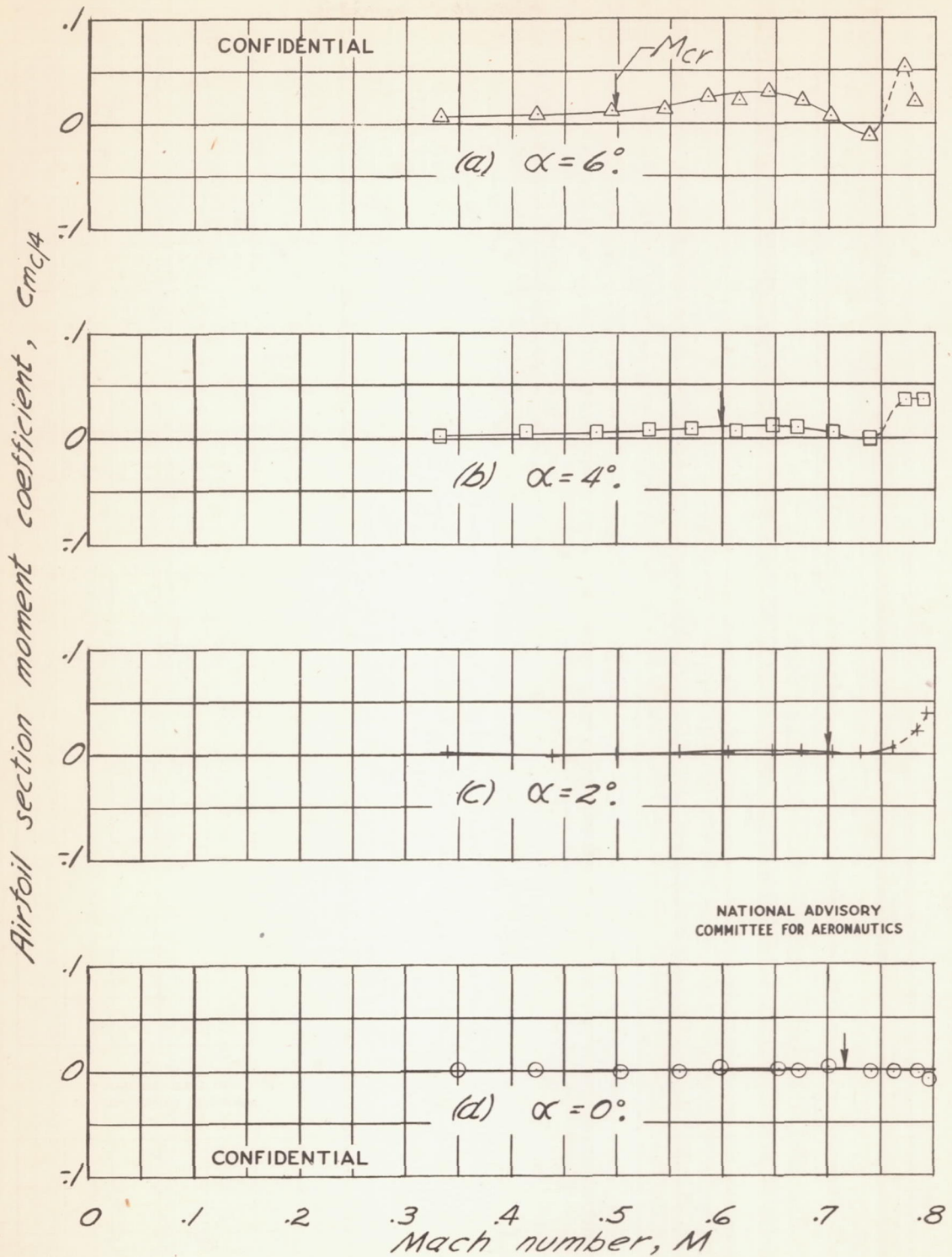

Figure 51.— Variation of section moment coefficient with Mach number for the NACA 66,2-215 airfoil.

Figure 52.— Variation of section moment
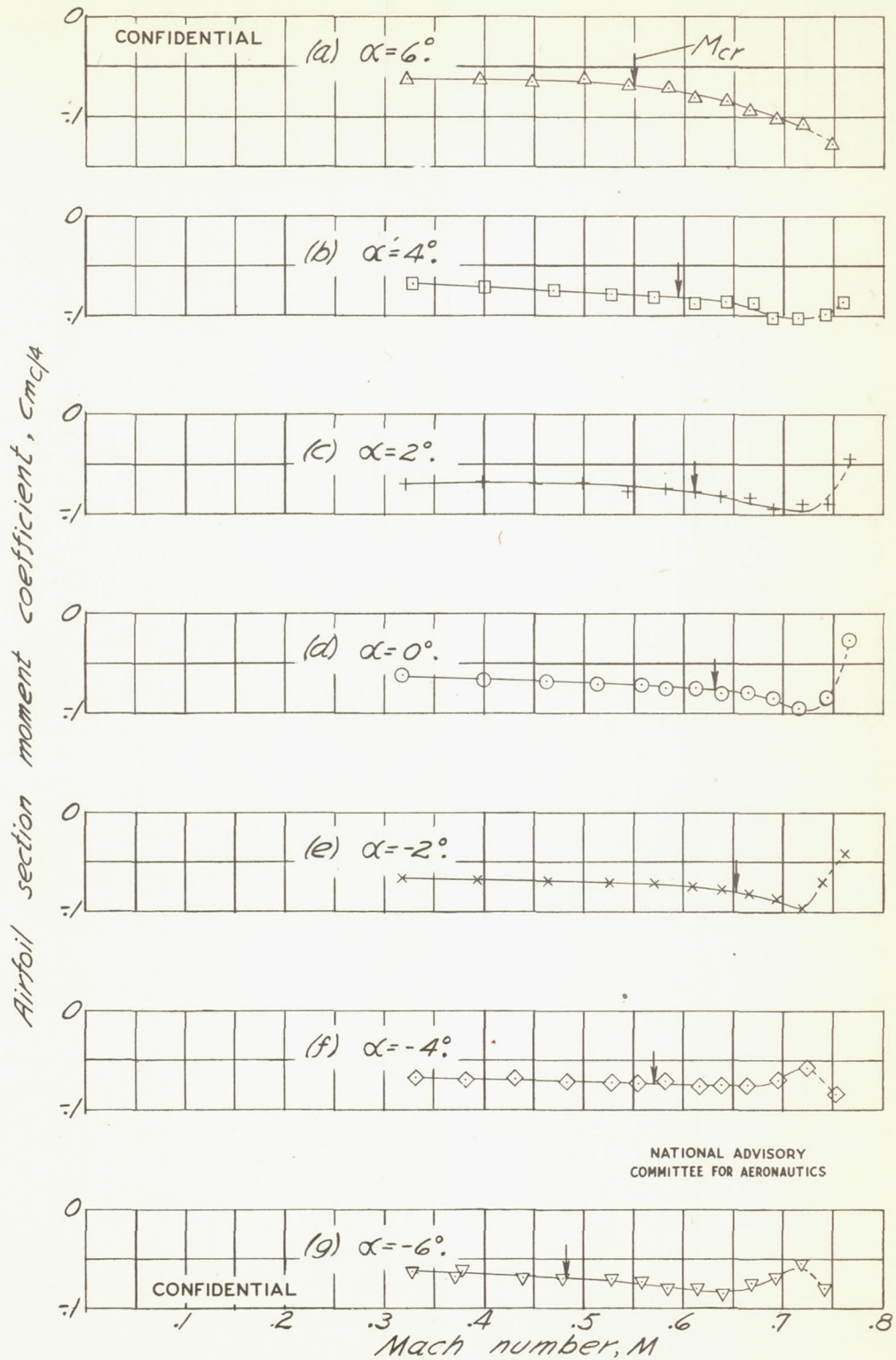coefficient with Mach number
for the NACA 66,2-015 airfoil.

Fig. 53   NACA RM No. L6L16

Figure 53.— Variation of section moment coefficient with Mach number for the NACA 65(216)-418 airfoil.
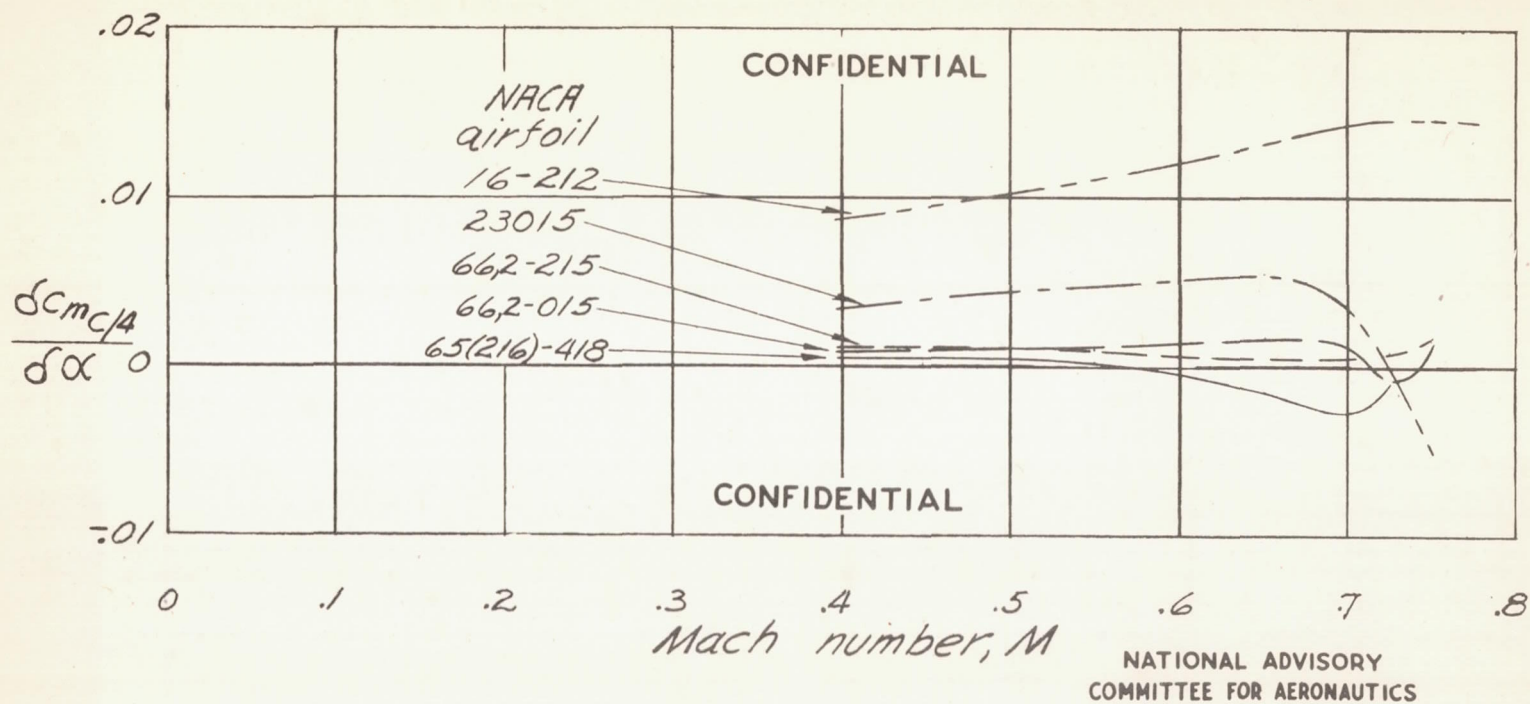
Figure 54. – Variation with Mach number of the slope of the curve of quarter-chord moment coefficient against angle of attack for each airfoil.
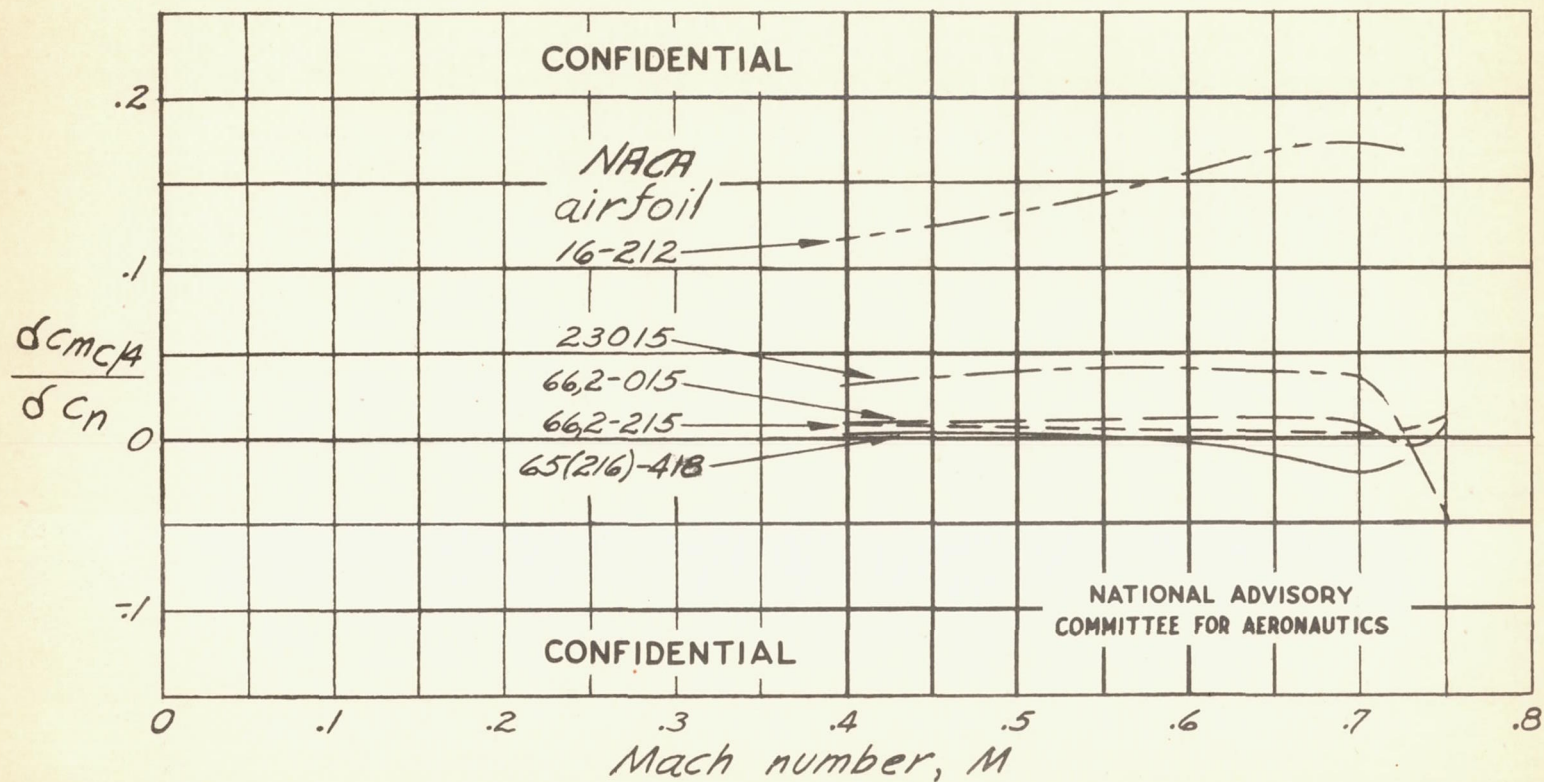
Fig. 54

Fig. 55

Figure 55.— Variation with Mach number of the slope of the curve of quarter-chord moment coefficient against normal-force coefficient for each airfoil.